Contents

Introduction and Historical background

The transmission of electric signals through metallic wires is one of the most important contributions to the development of modern technology. S.F.B. Morse invented the electric telegraph in 1838 and the first commercial telegraph line was erected in 1844, between New York, Baltimore and Washington. Nevertheless, at that time the theory of electric circuits was still at its dawn and hardly anything was known about the transmission of electric signals along conducting wires. The paper in which G. Kirchhoff formulated his well known laws has been published in 1845.

The rapid development of telegraphic signal transmission by means of overland lines and undersea cables (the first undersea cable was laid between France and England in 1851 and in 1853 the first transatlantic cable was installed) gave rise to a long series of theoretical investigations on the transmission of electrical signals through conducting wires.

Lord Kelvin (1855) studied the effects of transients in telegraphic signal transmission through long cables and formulated the first distributed parameter model for an electric cable. He assumed that the effects of magnetic field were negligible, and modelled the effects of electric induction by means of the per unit length capacitance of the cable and the lossy effects by means of the per unit length resistance, so deriving the well-known voltage diffusion equation (Lord Kelvin, 1855).

Shortly after G. Kirchhoff (1857), using Weber's electromagnetic theory (e.g., [1]), analysed the transmissions of electric signals through two wires with finite conductivity, including the effects of the magnetic field, and obtained what we can define as the first transmission line model [2]. He deduced that the electric signals propagate along the conductors with the same velocity as that which light propagates in the vacuum, several years before J. C. Maxwell published (1864) his fundamental paper demonstrating the electromagnetic nature of light [3].

Unfortunately, for reasons that are still not fully clear, Kirchhoff's work has

never been widely acknowledged and is even today largely unknown. There is an interesting work by G. Ferraris (1872) in which Kirchhoff's model is reviewed and studied in depth [4].

O. Heaviside $(1881 - 1887)$ was the first to study the "guided" propagation of electric signals along couples of rectilinear and parallel conducting wires, with finite conductivity, immersed in a lossy homogeneous dielectric, using Maxwell's electromagnetic theory. He developed the transmission line theory as it is still known today [5]. Hereafter the Heaviside transmission line model is called "standard" transmission line (STL) model.

G. Kirchhoff obtained his transmission line model starting with an integral formulation of the problem based on Weber's theory of electromagnetism. This theory is based on interaction at distance, described by two variables that can be considered as a forerunner of the electric scalar potential and the magnetic vector potential. Heaviside, instead, obtained his transmission line model starting from a formulation based directly on Maxwell's field theory under the assumption that the configuration of the electromagnetic field is quasi-TEM.

The STL model has since been extended to interconnects, even non-uniform ones, with many wires, in the presence of conducting planes and non-homogeneous dielectrics. The reader is referred to many excellent books and reviews existing in the literature for a complete and comprehensive treatment of the subject (e.g., [29], [30],[32]).

The STL model for conventional interconnects is based on the assumptions that:

- The interconnect quasi-parallel wires are metals whose electrical behaviour is governed by Ohm's law;

- the structure of the electromagnetic field surrounding the wires is of the quasi-TEM type with respect to the wire axis;

- the total current flowing through each transverse section is equal to zero.

A transverse electromagnetic (TEM) field structure is one in which the electric and magnetic fields in the space surrounding the conductors are transverse to the wire axis. The TEM fields are the fundamental modes of propagation of ideal multiconnected guiding structures, i.e. guiding structures with transverse section uniform along the wire axis, made by perfect conductors and embedded in a homogeneous medium (e.g., [29], [30],[32]).

In actual interconnects the electromagnetic field is never exactly of the TEM type. In ideal shielded guiding structures, high order non-TEM modes with discrete spectra can propagate as well as the TEM fundamental modes. In unshielded guiding structures there are also non-TEM propagating modes

with continuous spectra. Actual guiding structures are most frequently embedded in a transversally non homogeneous medium, and thus TEM modes cannot exist. However, even if the medium were homogeneous, due to the losses, the guiding structure could not support purely TEM modes. Furthermore, the field structure is complicated by the influence of non-uniformities present along the axis of the guiding structures (bends, crossovers, etc.). However, when the cross-sectional dimensions of the guiding structure are smaller than the smallest characteristic wavelength of the electromagnetic field propagating along it, the transverse components of the electromagnetic field give the "most significant" contribution to the overall field and to the resulting terminal voltages and currents (e.g., [6]). In other words, we have that the structure of the electromagnetic field is said to be of quasi-TEM type.

Nowadays, the speed of electronic signals is growing rapidly due to market requirements and to progress in technology, e.g. allowing switching times below 1 ns. Because of such high speed signals the distance between the wires of interconnects existing at various levels in an electronic circuit may become comparable with the smallest characteristic wavelength of the signal themselves. As a consequence high frequency effects such as dispersion and radiation losses are no more negligible and there is the need of a new model to describe the propagation of the signals along the interconnects.

Several efforts have been made to obtain generalized transmission line models from a full-wave analysis based on integral formulations to overcome the restrictions of the STL model [7, 8, 9, 10, 11, 12, 13, 14].

Start point and aim of the thesis

Recently the Professors Maffucci A., Miano G., Villone F., [23, 24, 25] have proposed an "enhanced" transmission line (ETL) model derived from a full-wave analysis based on an integral formulation of the electromagnetic field equations, which has the same simplicity and structure as the STL transmission line model. The ETL model describes the propagation along cylindrical cables in homogeneous dielectric, in frequency ranges where the STL model fails, takes into account the shape effects of the transverse cross-section of the interconnect wires and reduces to the STL model in the frequency ranges where the distance between wires is electrically short.

Specifically, the ETL model allows to forecast phenomena that the STL model cannot foresee, such as the distortion introduced by the non-local nature of the electromagnetic interaction along the conductors, and the attenuation due to radiation losses in the transverse direction. The ETL model considers thick quasi-perfect conducting wires and evaluates correctly the kernel that shows the logarithmic singularity that is typical of the surface distributions. Such a singularity plays a very important role in the radiation problems, e.g., it may regularise the numerical models (e.g., [15, 16]). The approach on which the ETL model is based bears a resemblance to the Kirchhoff approach [2]. The ETL model has been formulated, in origin, for study only the propagation of the differential mode on two conductor in homogeneous dielectric.

The aim of this thesis is extend the ETL model to take in account multiconductors buried in a stratified dielectric media and to describe both the propagation of the differential mode and of the common mode and the crosstalk in order to study the behaviour of the modern high-speed VLSI interconnects. Two different ways are possible in order to take in account the dielectric media, we can introduce in the formulation as other unknown the polarisation current in the dielectric media or we can compute the Green's function of the dielectric slab. The ETL model is developed in order to have full-wave results with a computational cost comparable with the STL model, then we need to

discard the first way because produce a big increase of the computational cost due to the need of discretize the dielectric media. In this thesis is showed as is possible include this kind of media in the ETL model with a very low increase of the computational cost, the most popular approaches to compute the Green's functions [36], [35],[37], [34] are exposed and a method to decrease furtherly the cost of the method using an approximated form of this functions [35] is proposed and validated with commercial simulator. As very important product of this research activity, we can use the ETL model to show the effect of the unwanted TM and TE mode (associate to power loss) because we can turn on and off the dynamic part of the Green's functions. The ETL model for VLSI interconnections exposed in this thesis is able to simulate multiconductor interconnections of practical interest and can describe accurately the crosstalk and the common mode propagation that are associated at noise on the victim lines and radiation loss in a frequency range where the STL model fails.

This thesis is organised as follow:

Chapter 1 Integral relations for the potentials and the field/circuit problem;

Chapter 2 Generalisation of the ETL model at the case of multiconductors buried in inhomogeneous medium;

Chapter 3 Numerical implementation of the method and the principal approaches for evaluate the Green functions of stratified media;

Chapter 4 Numerical results for two cylindrical cables in homogeneous media are compared with numerical and analytical full-wave solutions;

Chapter 5 Numerical results for microstrip interconnections are compared with two numerical full-wave solutions;

Chapter 1

General formulation

1.1 Integral relation

In this thesis, we consider electric conductors buried in an inhomogeneous dielectric as showed in figure:
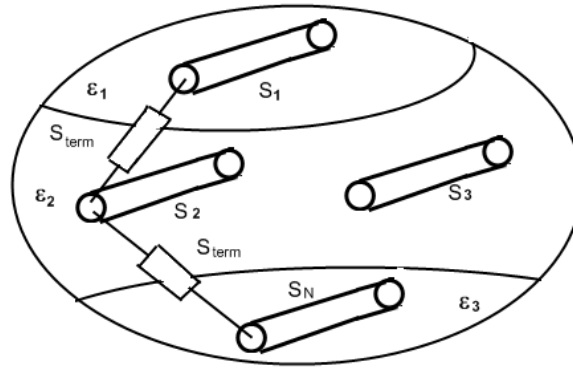
Figure 1.1: conductors buried in inhomogeneus dielectric

We assume that the time dependencies of all the fields are $\exp(i\omega t)$ where ω is the radiant frequency. We suppose that the geometrical dimensions are such that the current density is mainly located on the conductor surfaces then the sources of the electromagnetic field are the (superficial) current and charge densities J_s and σ_s , which must satisfy the *charge conservation law* :

$$\nabla_s \cdot \mathbf{J}_s + i\omega\sigma_s = 0 \qquad (1.1)$$

where (∇_s) is the surface divergence operator defined as $(\nabla - \hat{n}\frac{\partial}{\partial n})$.
The *Faraday-Neumann law* relates the electric to the magnetic field as:

$$\nabla \times \mathbf{E} = -i\omega\mathbf{B} \qquad (1.2)$$

In order to impose the solenoidality of $\mathbf{B}$ we can define a *magnetic vector potential* $\mathbf{A}$ like[1]:

$$\mathbf{B} = \nabla \times \mathbf{A} \tag{1.3}$$

using this definition in (1.2)we have:

$$\nabla \times (\mathbf{E} + i\omega\mathbf{A}) = 0 \tag{1.4}$$

that can be automatically satisfied[2] if we define an *electric scalar potential* φ such that:

$$\mathbf{E} = -i\omega\mathbf{A} - \nabla\varphi \tag{1.5}$$

The potentials $\mathbf{A}$ and φ are not uniquely defined, unless a suitable gauge condition is imposed, as for instance the so-called *Lorenz gauge*, that will be used in the present derivation:

$$\nabla \cdot \mathbf{A} + i\omega\varepsilon_r\varepsilon_0\mu_0\varphi = 0 \tag{1.6}$$

where ε_r is the relative dielectric constant of the embedding material and ε_0 and μ_0 are the dielectric constant and the magnetic permeability in the vacuum space. Is important to note that this condition can be imposed when the dielectric is homogeneous, instead on the discontinuity interfaces we need to impose the continuity of the tangent component of the fields. The gauge condition and the field continuity are imposed in the Green's functions.
The sources J_s and σ_s may be related to the potentials through the Green functions defined for the domain of interest:

$$\mathbf{A}\left(\mathbf{r}\right) = \mu_0 \iint\limits_{S} \mathbf{G}_A(\mathbf{r},\mathbf{r}')J_s(\mathbf{r}')dS' + \mathbf{A}^*_{EXT}\left(\mathbf{r}\right) \tag{1.7}$$

$$\varphi\left(\mathbf{r}\right) = \frac{1}{\varepsilon_0} \iint\limits_{S} G_\varphi(\mathbf{r},\mathbf{r}')\sigma_s(\mathbf{r}')dS' + \varphi^*_{EXT}\left(\mathbf{r}\right) \tag{1.8}$$

where S represents the union of all the N conductor surfaces ($S = \bigcup_{k=1,\cdots,N} S_k$) and $\mathbf{A}^*_{EXT}\left(\mathbf{r}\right)$, $\varphi^*_{EXT}\left(\mathbf{r}\right)$ are the contributes to the potential due at the charge and current present in the device connected at the interconnect, $\mathbf{G}_A$ and G_φ are the Green's functions that take in account the inhomogeneous medium hence we can avoid to discretize it. In order to close the problem we need to impose the boundary condition on the conductor, if the conductors are perfect we have to impose:

$$\mathbf{E} \times \hat{n} = 0|_{S_k} \rightarrow (-i\omega\mathbf{A} - \nabla\varphi) \times \hat{n} = 0|_{S_k} \tag{1.9}$$

---

[1] $\nabla \cdot \mathbf{B} = \nabla \cdot (\nabla \times \mathbf{A}) = 0$
[2] $\nabla \times (\nabla\varphi) = 0$

if the conductors have an ohmic behaviour , the boundary condition on the conductor will be:

$$\mathbf{E} \times \hat{n}|_{S_k} = \zeta_k \mathbf{J}_s \times \hat{n}|_{S_k} \rightarrow (-i\omega\mathbf{A} - \nabla\varphi) \times \hat{n}|_{S_k} = \zeta_k \mathbf{J}_s \times \hat{n}|_{S_k} \qquad (1.10)$$

where ζ_k is the surface impedance of the k-th conductor that take in account the ohmic losses. For high-frequency operating conditions, for instance, it reduces to the well-known *Leontovich expression*

$$\zeta_k = \eta_k \frac{1+i}{\delta_k} \qquad (1.11)$$

where η_k and δ_k are, respectively, the conductivity and the penetration depth of the k-th conductor.
Is important to note that using the integral relations (1.7), the *Sommerfeld radiation condition* is automatically imposed because we have the sources only at the finite then we can't have reflected energy from the infinity.

1.2 The field/circuit coupling problem

The *circuit theory* say that a component is completely describe through a relations between the terminal currents and the voltages, this theory provide correct results if the characteristic dimensions of the components are small compared to the smallest wavelength in the signal. In the case of the interconnects, this condition is not satisfied and in principle the wave propagation can be described only using the *field theory*, we need to match this description with the circuit description of the terminal components. To do this we have to derive a multi-port representation of the interconnect, that can be used with the circuit description of the rest of the circuit. Hence, we assume that it would be possible to characterise it regardless of the actual devices on which it is terminated. In other words, the terminal elements are taken into account only through the relations that they impose on the terminal currents and voltages, but the sources located on the components are neglected in computing the potentials (1.7) then we suppose that:

$$\mathbf{A}\,(\mathbf{r}) \approx \mu_0 \iint\limits_S \mathbf{G}_A(\mathbf{r}|\mathbf{r}')J_s(\mathbf{r}')dS' \qquad (1.12)$$

$$\varphi\,(\mathbf{r}) \approx \frac{1}{\varepsilon_0} \iint\limits_S G_\varphi(\mathbf{r}|\mathbf{r}')\sigma_s(\mathbf{r}')dS' \qquad (1.13)$$

This is a crucial point in the field/circuit coupling problem. This condition is approximately satisfied if the characteristic dimensions of the terminal devices are small compared to the interconnect length.

Anyway, as a consequence of this approximation, the potentials in (1.12) and (1.13) do not wholly satisfy the Lorenz gauge condition. However,it is easy to verify that, starting from (1.7) and (1.6)

$$\nabla \cdot \mathbf{A} + i\omega\varepsilon_r\varepsilon_0\mu_0\varphi = -\nabla \cdot \mathbf{A}^*_{EXT} - i\omega\varepsilon_r\varepsilon_0\mu_0\varphi^*_{EXT} \qquad (1.14)$$

The two right-hand terms of this expression are negligible only if the dimension of the terminal device is small respect the length of the interconnect.

Conversely, when the assumption does not hold, there is no way to separate the behaviour of the interconnect from that of terminal devices and the electromagnetic system has to be analysed as a whole.

Chapter 2

TL formulation

2.1   TM type field

The first fundamental assumption is that the surface current density is mainly directed along $\hat{x}$: $\mathbf{J}_s = J_x \hat{x}$. In other words we neglect any transverse component of the current density, taking into account only the longitudinal one. This assumption is well-founded when the interconnect length is infinite and only the fundamental mode is excited. Even with an infinite length, high-order propagation modes may exhibit non-longitudinal current density components, hence this assumption defines an upper limit in the frequency range. The first consequence of this assumption is a drastic simplification of (1.12) and (1.13).

We need to distinguish two cases:

1) The conductors are buried in an homogeneous dielectric, the magnetic vector potential (1.12) and (1.13) is directed only along $\hat{x}$

$$\mathbf{A}\left(\mathbf{r}\right) = \mu_0 \iint\limits_{S} \begin{pmatrix} G_A^{xx} & 0 & 0 \\ 0 & G_A^{xx} & 0 \\ 0 & 0 & G_A^{xx} \end{pmatrix} \begin{bmatrix} J_x(\mathbf{r}') \\ 0 \\ 0 \end{bmatrix} dS' \tag{2.1}$$

then there is only the A_x component:

$$A_x\left(\mathbf{r}\right) = \mu_0 \iint\limits_{S} G_A^{xx}(\mathbf{r}|\mathbf{r}') J_x(\mathbf{r}') dS' \tag{2.2}$$

and so the magnetic field is *rigorously* of TM type indeed:

$$\mathbf{B} = \nabla \times \begin{bmatrix} A_x \\ 0 \\ 0 \end{bmatrix} \rightarrow B_z = 0 \tag{2.3}$$

2) The conductors are buried in a multilayered media.
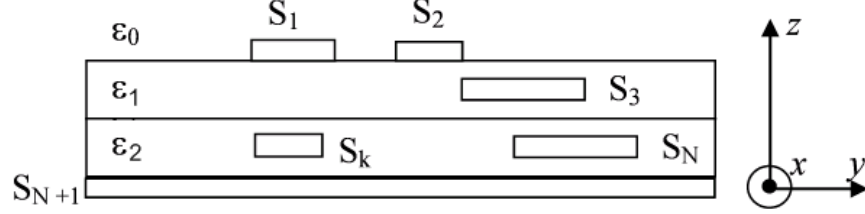
Figure 2.1: Generic cross-section of a multilayered interconnect

Since the layers properties are assumed to change only along $\hat{z}$ direction (see Figure 2.1), $\mathbf{G}_A$ has the structure

$$\mathbf{G}_A = \begin{bmatrix} G_{xx} & 0 & G_{zx} \\ 0 & G_{yy} & G_{zy} \\ G_{zx} & G_{zy} & G_{zz} \end{bmatrix} \tag{2.4}$$

then the magnetic vector potential (1.12) is:

$$\mathbf{A}\left(\mathbf{r}\right) = \mu_0 \iint\limits_S \begin{pmatrix} G_A^{xx} & 0 & G_A^{xz} \\ 0 & G_A^{yy} & G_A^{yz} \\ G_A^{zx} & G_A^{zy} & G_A^{zz} \end{pmatrix} \begin{bmatrix} J_x \\ 0 \\ 0 \end{bmatrix} dS' \tag{2.5}$$

hence

$$A_x(\mathbf{r}) = \mu_0 \iint\limits_S G_A^{xx}(\mathbf{r}|\mathbf{r}')J_x(\mathbf{r}')dS' \tag{2.6}$$

$$A_z(\mathbf{r}) = \mu_0 \iint\limits_S G_A^{zx}(\mathbf{r}|\mathbf{r}')J_x(\mathbf{r}')dS' \approx 0 \tag{2.7}$$

hence, there is also the A_z component but, in practical case, this component are negligible respect the A_x component,then we suppose that $A_z \approx 0$, so the magnetic field is *approximately* of TM type.

In this conditions, it is uniquely defined the voltage between any couple of points lying on a plane $x = const$.

$$V\left(x\right) = \int_\gamma \mathbf{E} \cdot d\mathbf{l} \quad 0 \leq x \leq l. \tag{2.8}$$

2.2 The first governing equation

The second assumption is that the current and charge densities have a spatial dependence of separable type:

$$J_s\left(\mathbf{r}\right)|_{\mathbf{r}\in S_k} = I_k\left(x\right)F_k'\left(s_k\right), \quad \sigma\left(\mathbf{r}\right)|_{\mathbf{r}\in S_k} = Q_k\left(x\right)F_k''\left(s_k\right) \qquad (2.9)$$

where $I_k(x)$ and $Q_k(x)$ are the total current and p.u.l. charge associated to the conductor, F_k' and F_k'' are shape functions dimensionally homogeneous with m^{-1} , describing the distribution of currents and charges along the contour l_k and s_k is the curvilinear abscissa in the transverse plane. In other words, we are assuming that only the total current $I_k(x)$ and p.u.l. charge $Q_k(x)$ vary along x, whereas the spatial distributions of current and charge densities are independent on x. Imposing the charge conservation law (1.1) on the k-th conductor and using (2.9) we obtain

$$\frac{dI_k\left(x\right)}{dx}F_k'\left(s_k\right) + i\omega Q_k\left(x\right)F_k''\left(s_k\right) = 0 \qquad (2.10)$$

which yields:

$$F_k'\left(s_k\right) = F_k''\left(s_k\right) = F_k\left(s_k\right) \qquad (2.11)$$

$$\frac{dI_k\left(x\right)}{dx} + i\omega Q_k\left(x\right) = 0 \qquad (2.12)$$

The shape functions for the charge and current distributions must be the same. If we impose the following normalization condition:

$$\oint_{l_k} F_k\left(\mathbf{s}_k\right)d\mathbf{s}_k = 1 \qquad (2.13)$$

then the current I_k and the p.u.l. charge Q_k are obtained by integrating (2.9) along l_k. With the position (2.9) the problem may be solved by separating the transverse and longitudinal behaviour of the current and charge distributions. When the characteristic transverse dimensions of the conductors are electrically short and the interconnect is geometrically long, the transverse behaviour $F_k(s_k)$ is obtained by solving once for all a quasi-static 2D problem in the transverse plane.

This assumption imposes the high-frequency validity limit for the ETL model, but produce a drastic reduction of the computational cost of the method.
Eq. (2.12) may be written for every conductor, introducing the numerical vectors $\mathbf{I}\left(x\right) = \left\{I_k\left(x\right)\right\}_{k=1..N}$ and $\mathbf{Q}\left(x\right) = \left\{Q_k\left(x\right)\right\}_{k=1..N}$:

$$\frac{d\mathbf{I}\left(x\right)}{dx} + i\omega\mathbf{Q}\left(x\right) = 0 \qquad (2.14)$$

This is the first of the two governing equations for any transmission line model.

2.3   The second governing equation

Let us now focus on the relation between the voltage and p.u.l. magnetic flux. Let a_k indicates a characteristic dimension of the cross-section of the k-th conductor and let $a = max_k(a_k)$: assuming operating conditions such that $ka \ll 1$ it is possible to approximate at any abscissa x the values of $\mathbf{A}(x,y,z)$ and $\varphi(x,y,z)$ on the surfaces Σ_k with their average values along the conductor cross-sections contours l_k, say $\tilde{A}_k(x)$ and $\tilde{\varphi}_k(x)$.

$$\tilde{A}_k(x) = \frac{1}{c_k} \oint_{l_k} A_x(x,y,z)d\mathbf{s}_k \tag{2.15}$$

$$\tilde{\varphi}_k(x) = \frac{1}{c_k} \oint_{l_k} \varphi(x,y,z)d\mathbf{s}_k \tag{2.16}$$

using this average values, the (1.10) become:

$$\left(-i\omega \tilde{A}_k(x) - \frac{d}{dx}\tilde{\varphi}_k(x) \right) = Z_s^{kk}(i\omega)I_k(x) \tag{2.17}$$

where

$$Z_s^{kk}(i\omega) = \frac{1}{c_k} \oint_{l_k} \zeta_s^k(\mathbf{s}_k)F'(\mathbf{s}_k)d\mathbf{s}_k \tag{2.18}$$

If the conductor are cylindrical and the proximity is negligible the (2.18) reduce to $Z_s^{kk}(i\omega) = \frac{\zeta_s^k}{\pi a_k}$. As already pointed out, it is possible to define uniquely the voltage between any two pair of points lying on a plane x = const. If we assume the (N+1)th conductor as ground reference, we may introduce the grounded mode voltage of the k-th conductor as follows

$$V_k(x) = \tilde{\varphi}_k(x) - \tilde{\varphi}_{N+1}(x) \tag{2.19}$$

The p.u.l. magnetic flux linked to a closed loop connecting the k-th conductor and the ground one in the plane y-z may be expressed as

$$\Phi_k(x) = \tilde{A}_k(x) - \tilde{A}_{N+1}(x) \tag{2.20}$$

Let us introduce the vectors $\mathbf{V}(x) = \{V_k(x)\}_{k=1..N}$ and $\mathbf{\Phi}(x) = \{\Phi_k(x)\}_{k=1..N}$ using (2.19) and (2.20) in (2.17) we obtain

$$-\frac{d\mathbf{V}(x)}{dx} = i\omega\mathbf{\Phi}(x) + Z_s(i\omega)\mathbf{I}(x) \tag{2.21}$$

where $Z_s(i\omega)$ is a diagonal matrix with $Z_s^{kk}(i\omega)$ on the diagonal.
This is the second governing equations for any transmission line model.

2.4   The ETL constitutive relations

Using the assumptions (2.9) in (2.15) we have:

$$\tilde{A}_k(x) = \mu_0 \frac{1}{c_k} \oint_{l_k} \sum_n \iint_{S_n} G_A^{xx}(\mathbf{r}|\mathbf{r}') I_n(x') F_n(\mathbf{s}_n) \, dS' d\mathbf{s}_k \qquad (2.22)$$

$$\tilde{\varphi}_k(x) = \frac{1}{\varepsilon_0} \frac{1}{c_k} \oint_{l_k} \sum_n \iint_{S_n} G_\varphi(\mathbf{r}|\mathbf{r}') Q_n(x') F_n(\mathbf{s}_n) \, dS' d\mathbf{s}_k \qquad (2.23)$$

then we can split the surface integral in a linear integral on the contour l_n and an integral on the x direction

$$\tilde{A}_k(x) = \mu_0 \frac{1}{c_k} \oint_{l_k} \sum_n \oint_{l_n} \int_0^l G_A^{xx}(\mathbf{s}_n; \mathbf{s}_k; x - x') I_n(x') F_n(\mathbf{s}_n) \, d\mathbf{s}_n dx' d\mathbf{s}_k \quad (2.24)$$

$$\tilde{\varphi}_k(x) = \frac{1}{\varepsilon_0} \frac{1}{c_k} \oint_{l_k} \sum_n \oint_{l_n} \int_0^l G_\varphi(\mathbf{s}_n; \mathbf{s}_k; x - x') Q_n(x') F_n(\mathbf{s}_k) \, d\mathbf{s}_n dx' d\mathbf{s}_k \quad (2.25)$$

Changing the integration order we can write

$$\tilde{A}_k(x) = \mu_0 \sum_n \int_0^l \left(\frac{1}{c_k} \oint_{l_k} \oint_{l_n} G_A^{xx}(\mathbf{s}_n; \mathbf{s}_k; x - x') F_n(\mathbf{s}_n) \, d\mathbf{s}_n d\mathbf{s}_k \right) I_n(x') \, dx'$$

$$\qquad (2.26)$$

$$\tilde{\varphi}_k(x) = \frac{1}{\varepsilon_0} \sum_n \int_0^l \left(\frac{1}{c_k} \oint_{l_k} \oint_{l_n} G_\varphi(\mathbf{s}_n; \mathbf{s}_k; x - x') F_n(\mathbf{s}_n) \, d\mathbf{s}_n d\mathbf{s}_k \right) Q_n(x') \, dx'$$

$$\qquad (2.27)$$

hence, using the position (2.20) and (2.19) these relations may be obtained from (1.12) and (1.13):

$$\mathbf{\Phi}(x) = \mu_0 \int_0^l \mathbf{H}_I(x - x') \mathbf{I}(x) dx' \qquad (2.28)$$

$$\mathbf{V}(x) = \frac{1}{\varepsilon_0} \int_0^l \mathbf{H}_Q(x - x') \mathbf{Q}(x) dx' \qquad (2.29)$$

These constitutive relations are spatial convolutions, hence their meaning is straightforward: in the general case the value of the p.u.l. magnetic flux (the

voltage) at a given abscissa x depends on the whole distribution of the current intensity (p.u.l electric charge) along the line. The kernels in (2.28) and (2.29) are matrices whose entries are:

$$
H_I^{nk}(\zeta) = \frac{1}{c_k} \oint_{l_k} \oint_{l_n} G_A^{xx}(\mathbf{s}_n; \mathbf{s}_k; \zeta) F_n(\mathbf{s}_n) \, d\mathbf{s}_n d\mathbf{s}_k +
$$
$$
- \frac{1}{c_{N+1}} \oint_{l_{N+1}} \oint_{l_n} G_A^{xx}(\mathbf{s}_n; \mathbf{s}_k; \zeta) F_n(\mathbf{s}_n) \, d\mathbf{s}_n d\mathbf{s}_k \tag{2.30}
$$

$$
H_Q^{nk}(\zeta) = \frac{1}{c_k} \oint_{l_k} \oint_{l_n} G_\varphi(\mathbf{s}_n; \mathbf{s}_k; \zeta) F_n(\mathbf{s}_n) \, d\mathbf{s}_n d\mathbf{s}_k +
$$
$$
- \frac{1}{c_{N+1}} \oint_{l_{N+1}} \oint_{l_n} G_\varphi(\mathbf{s}_n; \mathbf{s}_k; \zeta) F_n(\mathbf{s}_n) \, d\mathbf{s}_n d\mathbf{s}_k \tag{2.31}
$$

When the N+1 term in (2.30) and (2.31) is take in account in the Green's function then the kernels are simplified as

$$
H_I^{nk}(\zeta) = \frac{1}{c_k} \oint_{l_k} \oint_{l_n} G_A^{xx}(\mathbf{s}_n; \mathbf{s}_k; \zeta) F_n(\mathbf{s}_n) \, d\mathbf{s}_n d\mathbf{s}_k \tag{2.32}
$$

$$
H_Q^{nk}(\zeta) = \frac{1}{c_k} \oint_{l_k} \oint_{l_n} G_\varphi(\mathbf{s}_n; \mathbf{s}_k; \zeta) F_n(\mathbf{s}_n) \, d\mathbf{s}_n d\mathbf{s}_k \tag{2.33}
$$

The system of Eqs.(2.14),(2.21),(2.28) and (2.29), represents a generalised transmission line model: in the following we will refer to it as the enhanced transmission line (ETL) model. The 3D full-wave problem has been recast in a transverse quasi-static 2D problem and a 1-D propagation problem. The first problem is solved once for all and provides the source distributions $F_k(\mathbf{s}_k)$ along the conductor contours. The 1D propagation problem provides, instead, the distributions of voltages, currents, p.u.l. charge and magnetic flux along the line axis.

2.5 The STL constitutive relations

Letting the frequency go to zero and the interconnect length go to infinity, it is possible to prove that the kernels in (2.32)-(2.33) have a quasi-impulsive behaviour respect to ζ [24] then:

$$
\mathbf{\Phi}(x) = \mu_0 \int_0^l \mathbf{H}_I(x - x') \mathbf{I}(x) dx' \approx \mu_0 \left(\int_0^{+\infty} \mathbf{H}_I(x') dx' \right) \mathbf{I}(x) \tag{2.34}
$$

$$
\mathbf{V}(x) = \frac{1}{\varepsilon_0} \int_0^l \mathbf{H}_Q(x - x') \mathbf{Q}(x) dx' \approx \frac{1}{\varepsilon_0} \left(\int_0^{+\infty} \mathbf{H}_Q(x') dx' \right) \mathbf{Q}(x) \tag{2.35}
$$

hence we have the local relations

$$\mathbf{\Phi}(x) \approx \mu_0 \mathbf{H}_{I0} \mathbf{I}(x) = \mathbf{L}\mathbf{I}(x) \tag{2.36}$$

$$\mathbf{V}(x) \approx \frac{1}{\varepsilon_0} \mathbf{H}_{Q0} \mathbf{Q}(x) = \mathbf{C}^{-1} Q(x) \tag{2.37}$$

where $\mathbf{L} = \mu_0 \mathbf{H}_{I0}$ and $\mathbf{C} = (\frac{1}{\varepsilon_0} \mathbf{H}_{Q0})^{-1}$ are the p.u.l. inductance and capacitance matrices of the STL problem.

In conclusion, when the interconnect is enough long to neglect the effect of the finite length and the frequency is enough low to make the transverse dimensions electrically small the ETL model tends to the STL model:

$$-\frac{d\mathbf{V}(x)}{dx} = Z(i\omega)\mathbf{I}(x), \quad -\frac{d\mathbf{I}(x)}{dx} = Y(i\omega)\mathbf{V}(x) \tag{2.38}$$

where $Z(i\omega) = i\omega\mu_0 H_{I0}(\omega) + Z_s(i\omega), \quad Y(i\omega) = i\omega\varepsilon_0 H_{Q0}^{-1}(\omega)$ are the per-unit-length impedance and admittance matrices.

2.6 The quasi-static 2D problem

The shape functions for the charge and the current can be founded solving once for all a quasi static 2D problem along the conductor contours in the additional hypothesis of geometrical long interconnect. The scalar potential depends solely on the spatial variable x

$$\varphi_k(x) \approx \frac{Q(x)}{\varepsilon_0} \sum_n \left(\oint_{l_n} g_\varphi(\mathbf{s}_n; \mathbf{s}_k) F_n(\mathbf{s}_n) \, d\mathbf{s}_n \right) \tag{2.39}$$

where $g_\varphi(\mathbf{s}_n; \mathbf{s}_k)$ is the quasi static Green's function and $\mathbf{s}_n, \mathbf{s}_k$ are, respectively, the source point and the observation point in the transverse section. ... ...

$$\frac{\varphi_k(x)}{Q(x)} = \frac{1}{\varepsilon_0} \sum_n \left(\oint_{l_n} g_\varphi(\mathbf{s}_n; \mathbf{s}_k) F_n(\mathbf{s}_n) \, d\mathbf{s}_n \right) \tag{2.40}$$

these equations are verified for every x

$$\alpha_k = \frac{1}{\varepsilon_0} \sum_n \left(\oint_{l_n} g_\varphi(\mathbf{s}_n; \mathbf{s}_k) F_n(\mathbf{s}_n) \, d\mathbf{s}_n \right) \tag{2.41}$$

where α_k are real dimensionless and unknown constants that have to be imposed in such away to satisfy the normalization conditions (2.13) in this way the shape functions $F_k(\mathbf{s}_k)$ are univocally determine.

A way to solve this problem, if we choose N+1 conductors as ground reference, is choose $\alpha_1^{(1)} = 1$, $\alpha_{j=2\cdots N}^{(1)} = 0$ and compute the shape function $F_1^{(1)}, F_2^{(1)}, \cdots, F_N^{(1)}$ from the integral problem (2.41), then evaluate the charge on the conductors as

$$Q_{j1} = \oint_{l_j} F_j^{(1)}(\mathbf{s}_j)d\mathbf{s}_j \neq 1 \tag{2.42}$$

hence these values are equal at the first row of the capacitance matrix C_{1j}, because we have choose unitary potential value, repeating this procedure for $\alpha_i^{(i)} = 1$, $\alpha_{j \neq i}^{(i)} = 0$ $i = 2, \cdots, N$ we can fill in all the capacitance matrix.

The shape functions, that we have found, don't satisfy the normalization condition (2.13), in order to do this we have to compute the coefficient α_k as follow:

$$\begin{bmatrix} \alpha_1 \\ \alpha_2 \\ \vdots \\ \alpha_N \end{bmatrix} = \begin{pmatrix} C_{11} & C_{12} & \cdots & C_{1N} \\ C_{21} & C_{22} & \cdots & C_{2N} \\ \cdots & \cdots & \cdots & \cdots \\ C_{N1} & C_{N2} & \cdots & C_{NN} \end{pmatrix} \begin{bmatrix} 1 \\ 1 \\ \vdots \\ 1 \end{bmatrix} \tag{2.43}$$

then with this value we can solve the integral problem (2.41) that provide the normalized shape functions that we need. As sub product of this procedure we have found the capacitance matrix of the structure, if we repeat all but with the free space Green's function we can found the capacitance matrix for only the conductor, using the relation

$$\mathbf{C}_{vuoto}\mathbf{L} = \epsilon_0\mu_0\mathbf{I} \tag{2.44}$$

where $\mathbf{I}$ is the identity matrix, we can compute the inductance matrix of the structure.

2.7   Mode conversion

A correct analysis of the mixed-mode propagation of differential and common mode currents along interconnects is of great interest in high-speed circuits. For instance, the accurate evaluation of the common-mode currents is a crucial point in the analysis of systems like printed circuit boards (PCB), because of their remarkable effect on the overall EMI performance. Although they may be even some order of magnitude lower than the differential mode currents, their effects may be comparable, for instance, in terms of radiated emissions [18]. In the PCBs the control of the emissions generated by the common-mode currents on the circuitry is one of the crucial points in the analysis of the EMI performance [20]-[22]. This is because the common-mode currents drive the interconnects in the so-called antenna-mode (the radiated fields generated

by such currents tend to sum up), while the differential-mode currents is the transmission-mode (the radiated fields tend to cancel each others). Usually the common-mode currents are due to unwanted effects: the presence of an external field, the coupling between differential and common mode currents due to asymmetric conductor cross-sections and non-ideal behaviour of the ground. In other cases the common-mode is not due to unwanted effect. In the differential signalling technique, a signal is defined as the difference between the signals of two conductors with respect to a third reference one, so that the performance is not affected by a floating reference. However, due to the presence of the ground, a common-mode solution may propagate. Let us consider the interconnect of Fig. 2.7, of total length l, made by two signal conductors and a ground plane.
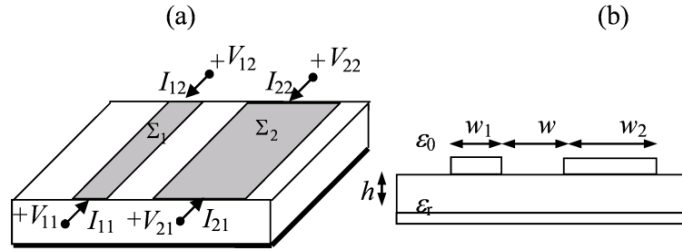
Figure 2.2: Coupled microstrip

In the *differential signalling technique* the signal is defined as the difference between the signals of the two conductors:

$$I_d(x) \equiv \frac{I_1(x) - I_2(x)}{2}, \quad V_d(x) \equiv V_1(x) - V_2(x). \qquad (2.45)$$

This propagating mode is known as the *differential mode*. The presence of the ground plane allows of course the interconnect to support a second mode, which is referred to as the *common mode*:

$$I_C(x) \equiv I_1(x) + I_2(x), \quad V_C(x) \equiv \frac{V_1(x) + V_2(x)}{2}. \qquad (2.46)$$

The grounded mode solution

$$\begin{bmatrix} \mathbf{V}_1 \\ \mathbf{V}_2 \end{bmatrix} = \begin{bmatrix} Z_{11} & Z_{12} \\ Z_{21} & Z_{22} \end{bmatrix} \begin{bmatrix} \mathbf{I}_1 \\ \mathbf{I}_2 \end{bmatrix} \qquad (2.47)$$

where the terminal voltages and currents are defined as $\mathbf{X}_1 = [X_1(0)\ X_2(0)]^T$, $\mathbf{X}_2 = [X_1(l)\ X_2(l)]^T$. A simple linear combination may lead to the mixed-mode

representation

$$\begin{bmatrix} \mathbf{V}_{M1} \\ \mathbf{V}_{M2} \end{bmatrix} = \begin{bmatrix} Z_{M11} & Z_{M12} \\ Z_{M21} & Z_{M22} \end{bmatrix} \begin{bmatrix} \mathbf{I}_{M1} \\ \mathbf{I}_{M2} \end{bmatrix} \tag{2.48}$$

where the terminal mixed-mode voltages and currents are defined as the above terminal voltages and currents, and

$$\begin{bmatrix} Z_{M11} & Z_{M12} \\ Z_{M21} & Z_{M22} \end{bmatrix} = \begin{bmatrix} \underline{\underline{B}} & \underline{\underline{0}} \\ \underline{\underline{0}} & \underline{\underline{B}} \end{bmatrix} \begin{bmatrix} Z_{11} & Z_{12} \\ Z_{21} & Z_{22} \end{bmatrix} \begin{bmatrix} \underline{\underline{A}}^{-1} & \underline{\underline{0}} \\ \underline{\underline{0}} & \underline{\underline{A}}^{-1} \end{bmatrix} \tag{2.49}$$

where $\underline{\underline{A}} = \begin{bmatrix} 1/2 & -1/2 \\ 1 & 1 \end{bmatrix}$ and $\underline{\underline{B}} = \begin{bmatrix} 1 & -1 \\ 1/2 & 1/2 \end{bmatrix}$

2.8 Scattering parameter

2.8.1 Scattering parameter, general definition

At high frequency is very difficult measure directly the impedance matrix because we need to open a terminal or close a terminal on a short circuit that can produce oscillating behaviour if active device are present, furthermore if very difficult to build broadband open or short circuit . The S parameter can be measured connecting the Device Under Test (DUT) at a transmission line (usually coaxial cable) whose ends are connected to a Vector Network Analyzer (VNA).[31]

The measurement setup can be modelled as
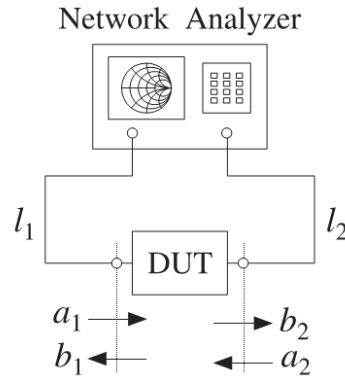
Figure 2.3: Measurement setup

we define a forward and backward wave respect the $\hat{x}$ direction as

$$a_k'(x) = \frac{V_k(x) + Z0 I_k(x)}{2\sqrt{Z_0}} \tag{2.50}$$

$$b_k'(x) = \frac{V_k(x) - Z0 I_k(x)}{2\sqrt{Z_0}} \tag{2.51}$$

for simplicity we consider the two port case, at the port 1 we can define

$$a_1 = a_1'(0) \tag{2.52}$$
$$b_1 = b_1'(0) \tag{2.53}$$

at the port 2 we can define [1]

$$a_2 = b_1'(l) \tag{2.54}$$
$$b_2 = a_1'(l) \tag{2.55}$$

then the scattering matrix are defined as

$$\begin{bmatrix} b_1 \\ b_2 \end{bmatrix} = \begin{bmatrix} S_{11} & S_{12} \\ S_{21} & S_{22} \end{bmatrix} \begin{bmatrix} a_1 \\ a_2 \end{bmatrix} \tag{2.56}$$

we can simply measure these parameters if we close a terminal on a matched load $Z_L = Z_0$, then there is no reflected wave $a_2 = 0$ and

$$S_{11} = \left. \frac{b_1}{a_1} \right|_{a_2=0} \tag{2.57}$$

$$S_{21} = \left. \frac{b_2}{a_1} \right|_{a_2=0} \tag{2.58}$$

close the DUT on a matched load that is the better work condition for the DUT.

2.8.2 S parameters, ETL model

We can reformulate the ETL model in order to compute directly the S parameters, indeed deriving the (2.50) we have

$$\frac{d\mathbf{a}'}{dx} = \frac{1}{2\sqrt{Z_0}} \left(\frac{d\mathbf{V}}{dx} + Z0 \frac{d\mathbf{I}}{dx} \right) \tag{2.59}$$

$$\frac{d\mathbf{b}'}{dx} = \frac{1}{2\sqrt{Z_0}} \left(\frac{d\mathbf{V}}{dx} - Z0 \frac{d\mathbf{I}}{dx} \right) \tag{2.60}$$

---

[1]note that the incident wave a_2 on the port 2 is in $-\hat{x}$ direction then is the backward wave defined in (2.50)

using (2.14),(2.21), we obtain

$$\frac{d\mathbf{a}'}{dx} = \frac{1}{2\sqrt{Z_0}} \left(-j\omega\mathbf{\Phi} - j\omega Z0\mathbf{Q} \right) \tag{2.61}$$

$$\frac{d\mathbf{b}'}{dx} = \frac{1}{2\sqrt{Z_0}} \left(-j\omega\mathbf{\Phi} + j\omega Z0\mathbf{Q} \right) \tag{2.62}$$

using (2.28) we have

$$\frac{d\mathbf{a}'}{dx} = \frac{1}{2\sqrt{Z_0}} \left(-j\omega\mu_0 \int_0^l \mathbf{H}_I(x-x')\mathbf{I}(x)dx' - j\omega Z0\mathbf{Q} \right) \tag{2.63}$$

$$\frac{d\mathbf{b}'}{dx} = \frac{1}{2\sqrt{Z_0}} \left(-j\omega\mu_0 \int_0^l \mathbf{H}_I(x-x')\mathbf{I}(x)dx' + j\omega Z0\mathbf{Q} \right) \tag{2.64}$$

from the definitions (2.59),(2.60) and the equation (2.29) we obtain

$$\mathbf{a}'(x) = \frac{1}{2\sqrt{Z_0}} \left(\frac{1}{\varepsilon_0} \int_0^l \mathbf{H}_v(x-x')\mathbf{Q}(x')dx' + Z0\mathbf{I}(z) \right) \tag{2.65}$$

$$\mathbf{b}'(x) = \frac{1}{2\sqrt{Z_0}} \left(\frac{1}{\varepsilon_0} \int_0^l \mathbf{H}_v(x-x')\mathbf{Q}(x')dx' - Z0\mathbf{I}(x) \right) \tag{2.66}$$

2.8.3 S parameters, mode conversion

Let us consider the structure of fig. 2.7, we can define on the port 1

$$a_1^{\mathbf{I}} = a_1'(0) \quad b_1^{\mathbf{I}} = b_1'(0) \quad a_2^{\mathbf{I}} = a_2'(0) \quad b_2^{\mathbf{I}} = b_2'(0)$$

on the port 2

$$a_1^{\mathbf{II}} = b_1'(l) \quad b_1^{\mathbf{II}} = a_1'(l) \quad a_2^{\mathbf{II}} = b_2'(l) \quad b_2^{\mathbf{II}} = a_2'(l)$$

using this definition the S matrix is

$$\begin{bmatrix} b_1^{\mathbf{I}} \\ b_2^{\mathbf{I}} \\ b_1^{\mathbf{II}} \\ b_2^{\mathbf{II}} \end{bmatrix} = \left[\begin{array}{cc|cc} S_{11} & S_{12} & S_{13} & S_{14} \\ S_{21} & S_{22} & S_{23} & S_{24} \\ \hline S_{31} & S_{32} & S_{33} & S_{34} \\ S_{41} & S_{42} & S_{43} & s_{44} \end{array} \right] \begin{bmatrix} a_1^{\mathbf{I}} \\ a_2^{\mathbf{I}} \\ a_1^{\mathbf{II}} \\ a_2^{\mathbf{II}} \end{bmatrix} \tag{2.67}$$

furthermore we can relate the 4-port single-ended scattering-matrix to the mixed-mode scattering matrix, using the definition proposed in [17]

$$\underline{\underline{S}}_M = \underline{\underline{M}}\,\underline{\underline{S}}\,\underline{\underline{M}}^{-1} \tag{2.68}$$

where

$$\underline{\underline{M}} = \frac{1}{\sqrt{2}} \begin{bmatrix} 1 & -1 & 0 & 0 \\ 0 & 0 & -1 & 1 \\ 1 & 1 & 0 & 0 \\ 0 & 0 & 1 & 1 \end{bmatrix} \tag{2.69}$$

Chapter 3

ETL, numerical implementation

3.1 ETL, Cylindrical cable, an analytical test case

Let us study the simple case of a straight pair in the vacuum space, made by two cylindrical perfect conductors of radius a. Let h_c be the center to center distance in the transverse plane (Fig.3.1) and l the total length. The example can be also used to analyse the case of a cylindrical conductor above a perfect ground plane. In vacuum the Green functions reduce to the function

$$G(\mathbf{r}) = \frac{e^{-ik\mathbf{r}}}{\mathbf{r}} \tag{3.1}$$

where $\mathbf{r}$ is the distance between the source and field points.
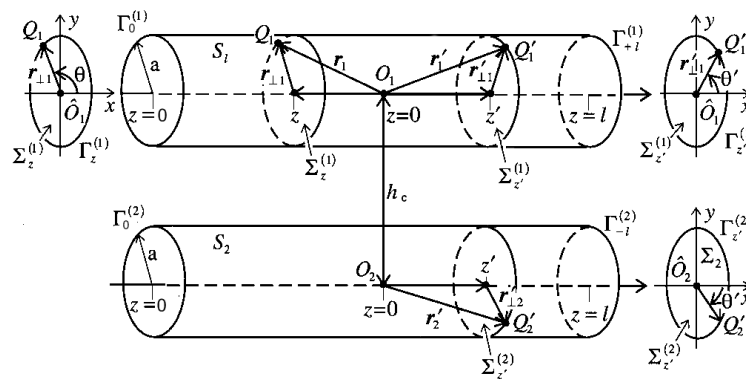
Figure 3.1: Cylindrical wires

in this case the (2.41) become

$$\alpha_1 = \frac{1}{\varepsilon_0} \left(\oint_{l_1} g_\varphi(\mathbf{s}_1; \mathbf{s}_1) F_1(\mathbf{s}_1)\, d\mathbf{s}_1 \right) + \left(\oint_{l_1} g_\varphi(\mathbf{s}_2; \mathbf{s}_1) F_2(\mathbf{s}_2)\, d\mathbf{s}_2 \right) \tag{3.2}$$

where $g_\varphi(\mathbf{r}) = -\frac{1}{2\pi}\ln \mathbf{r}$.

We consider the case of differential feed then the current on the conductor are equal and opposite $J_1 = -J_2 \rightarrow F_1 = -F_2$, using the geometry of the problem we have

$$\alpha_1 = \frac{1}{\varepsilon_0} 2a \left(\int_0^{2\pi} g_\varphi(|\mathbf{r}_{\perp 1} - \mathbf{r}'_{\perp 1}|) F_1(\theta')\, d\theta'_1 \right) - \left(\int_0^{2\pi} g_\varphi(|\mathbf{r}_{\perp 1} + h\hat{y} - \mathbf{r}'_{\perp 2}|) F_1(\theta')\, d\theta' \right) \tag{3.3}$$

this is a Fredholm integral equation of the first kind.

The $F_1(\theta)$ is the surface charge distribution in the transverse plane if the conductor are of infinite length and the linear charge density are $1 C/m$ for the first conductor and $-1 C/m$ for the second one, this a canonical problem and the solution is [33]

$$F_1(\theta) = \frac{1}{2\pi a} [F_-(\theta) - F_+(\theta)] \tag{3.4}$$

where [24]:

$$F_\pm(\theta) = \frac{a^2 \cos^2(\theta) \pm a \sin(\theta)\left[b \pm \left(h/2 + a\sin^2(\theta)\right)\right]^2}{a^2 \cos^2(\theta) + \left[b \pm \left(h/2 + a\sin^2(\theta)\right)\right]^2} \tag{3.5}$$

$$b = \sqrt{\left(\frac{h}{2}\right)^2 - a^2} \tag{3.6}$$

When considering widely separated conductors it results $F_1(\theta) = 1/(2\pi a)$ and it is possible to give a closed-form expression to the kernel (2.28) and (2.29), which are equal and may be split as the sum of a static and a dynamic term, $H = H_I = H_Q = H_{stat} + H_{dyn}$:

$$H_{stat}(\zeta) = \frac{1}{\pi^2} \frac{\kappa\left[m(\zeta)\right]}{R_s(\zeta)} - \frac{1}{2\pi} \frac{1}{R_m(\zeta)} \tag{3.7}$$

$$H_{dyn}(\zeta) = -\frac{ik}{\pi} \exp\left[-\frac{ikR_m(\zeta)}{2}\right] \mathrm{sinc}\left[\frac{kR_m(\zeta)}{2}\right] \tag{3.8}$$

Here $\kappa(m)$ is the *complete elliptic integral* of the first type, and

$$m(\zeta) = \frac{\zeta^2}{4a^2 + \zeta^2}, \quad R_m(\zeta) = \sqrt{h_c^2 + \zeta^2}, \quad R_s(\zeta) = \sqrt{4a^2 + \zeta^2} \tag{3.9}$$

The dynamic term depends on the frequency and vanishes as $\omega \to 0$. The static term is independent on frequency but shows a singularity of logarithmic type:

$$H_s\left(\zeta\right) \approx -\frac{1}{2a\pi^2}\ln\left(\zeta\right) \qquad for \quad \zeta \to 0 \tag{3.10}$$

This is the characteristic singularity associated with surface distribution and it is integrable. As already pointed out, if we consider infinitely-long lines and assume frequency operating conditions such that $h_c/\lambda \ll 1$, λ being the characteristic signal wavelength, $H(\zeta)$ reduces to a spatial Dirac pulse $H(\zeta) \to H_0\delta(\zeta)$, where

$$H_0 = \int\limits_{-\infty}^{\infty} H(x)dx = \frac{1}{\pi}\ln\left(\frac{h_c}{a}\right) \tag{3.11}$$

In this case the cylindrical pair is described by the classical telegrapher's equations for ideal two-conductor lines, and we retrieve the classical result:

$$L = \mu_0 H0 = \frac{\mu_0}{\pi}\ln\left(\frac{h_c}{a}\right) \tag{3.12}$$

$$C = \frac{\varepsilon_0}{H_0} = \frac{\varepsilon_0 \pi}{\ln\left(\dfrac{h_c}{a}\right)} \tag{3.13}$$

3.2 ETL, Coupled microstrip

A structure of great interest for high-speed electronic applications is the microstrip line: Figure 3.2 shows a simple example of a three conductor microstrip, made by two signal conductors on a dielectric layer and a ground plane the references for the voltages and currents are showed, note that the grounded modes are considered.
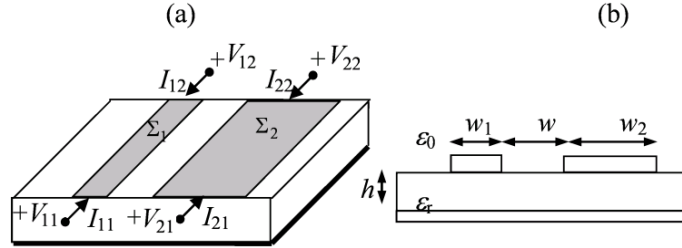
Figure 3.2: Coupled microstrip

From a qualitative point of view, the results highlighted in paragraph 3.1 still hold: the kernels (2.32)-(2.33) show a singularity of logarithmic type and the standard transmission line model may be obtained as a limit case of the generalised one.

3.2.1 The Green's function

In this case the kernels (2.32)-(2.33) are different, due to the dielectric influence, since we have to consider two different Green functions in (1.12)-(1.13). The Green function $\mathbf{G}_A$ involved in (1.12) is in general dyadic but in many practical applications the thickness of conductors t is small compared to their width w therefore the magnetic field is approximable with a TM type field, as already pointed out in the paragraph 2.1, hence the only component that we need is G_{xx}^A.

For the considered structure the Green functions may be evaluated in closed form in the spectral domain [34],[35],[36],[37] :

$$\tilde{G}_A^{xx}(k_\rho; z > 0 | z' > 0) = \frac{1}{2ik_{z0}} \left[e^{-ik_{z0}|z-z'|} + R_{TE} e^{-ik_{z0}(z+z')} \right] \tag{3.14}$$

$$\tilde{G}_\varphi(k_\rho; z > 0 | z' > 0) = \frac{1}{2ik_{z0}} \left[e^{-ik_{z0}|z-z'|} + (R_{TE} + R_q) e^{-k_{z0}(z+z')} \right] \tag{3.15}$$

where

$$R_{TE} = -\frac{r^{TE} + e^{-i2k_{zr}t}}{1 + r^{TE}e^{-i2k_{zr}t}};$$

$$R_q = \frac{2k_{z0}^2(1 - \varepsilon_r)(1 - e^{-i4k_{zr}t})}{(k_{zr} + k_{z0})(k_{zr} + \varepsilon_r k_{z0})(1 + r^{TE}e^{-i2k_{zr}t})(1 - r^{TM}e^{-i2k_{zr}t})}?$$

$$k_{z0} = \sqrt{k_0^2 - k_\rho^2}; \quad k_{zr} = \sqrt{\varepsilon_r k_0^2 - k_\rho^2}; \quad r^{TE} = \frac{k_{zr} - k_{z0}}{k_{zr} + k_{z0}}; \quad r^{TM} = \frac{k_{zr} - \varepsilon_r k_{z0}}{k_{zr} + \varepsilon_r k_{z0}}$$

The spatial domain functions are obtained by evaluating the Sommerfeld integrals [35]

$$G_A^{xx}(\rho; z, z') = \frac{1}{4\pi} \int\limits_{-\infty(SIP)}^{+\infty} \tilde{G}_A^{xx}(k_\rho) H_0^{(2)}(k_\rho \rho) k_\rho dk_\rho = S_0\{\tilde{G}_A^{xx}(k_\rho)\} \qquad (3.16)$$

$$G_\varphi(\rho; z, z') = \frac{1}{4\pi} \int\limits_{-\infty(SIP)}^{+\infty} \tilde{G}_\varphi(k_\rho) H_0^{(2)}(k_\rho \rho) k_\rho dk_\rho = S_0\{\tilde{G}_\varphi(k_\rho)\} \qquad (3.17)$$

where $H_0^{(2)}$ is the Hankel function of second kind and order 0, ρ is the distance in the plane xy, z and z' are, respectively, the horizontal positions of the observe and the source and SIP is an integration path in the first and third quadrant of the k_ρ complex plane that detours around the poles and the branch point of the argument.

Due to the slowly decaying and highly oscillating behaviour of the function to be integrated, the brute force numerical computation is time consuming.
A way to speed up the evaluation of the Sommerfeld integral is approximate the spectral domain Green's functions $\tilde{G}_A^{xx}(k_\rho)$ and $\tilde{G}_\varphi(k_\rho)$ in terms of certain functions for which Sommerfeld integrals can be obtained in closed form.
 Here we summarise the ideas at the base of the most popular algorithms (DCIM [35],[34], RFFM [36], TLSM [37])to do this task.
All the methods, that we'll show, first remove the asymptotic behaviour $\tilde{G}_{as}$ (see paragraph 3.2.2 for detail) of the Green's functions for $k_\rho \rightarrow \infty$ that dominate the near field interaction $\rho \rightarrow 0$, in order to improve the convergence of the fitting procedure of the remaining part done with the algorithm summarised in the next.

Discrete Complex Image Method (DCIM)

$\tilde{G} - \tilde{G}_{as}$ is approximated in terms of complex exponentials using the Generalised Pencil of Function Method (GPFM) as

$$\tilde{G} - \tilde{G}_{as} \approx \sum_{k=1}^{N} a_k e^{-b_k k_{zr}} \tag{3.18}$$

To obtain the spatial domain Green's function we can use the Sommerfeld Identity:

$$\frac{e^{-ikr_k}}{r_k} = \int\limits_{-\infty}^{+\infty} \frac{e^{ik_{zr}|z|}}{ik_{zr}} e^{-b_k k_{zr}} H_0^2(k_\rho \rho) k_\rho dk_\rho \tag{3.19}$$

where $r_k = \sqrt{\rho^2 - b_k^2}$ [1] then we have:

$$G \approx G_{as} + \sum_{k=1}^{N} a_k \frac{e^{-ikr_k}}{r_k} \tag{3.20}$$

In order to increase the convergence of this method, and have the correct behaviour for large distance, is needed to extract the poles of the spectrum domain green function that in the spatial domain give the TM/TE Surface Waves that dominate the far field behaviour:

$$\tilde{G} - \tilde{G}_{as} \approx \sum_{k=1}^{N} a_k e^{-b_k k_{zr}} + \sum_{k=1}^{N_{TE}} \frac{a_k^{TE}}{k_\rho^2 - (p_k^{TE})^2} + \sum_{k=1}^{N_{TM}} \frac{a_k^{TM}}{k_\rho^2 - (p_k^{TM})^2} \tag{3.21}$$

where $a^{TE}; a^{TM}$ and $p^{TE}; p^{TM}$ are, respectively, the residuals and the poles of the TE and TM Surface Wave. To obtain the spatial domain Green's function we can use the identity:

$$-\frac{j}{4} H_0^{(2)}(p\rho) = \int\limits_{-\infty(SIP)}^{+\infty} \frac{1}{k_\rho^2 - p^2} H_0^2(k_\rho \rho) k_\rho dk_\rho \tag{3.22}$$

then we have:

$$G \approx G_{as} + \sum_{k=1}^{N} a_k \frac{e^{-ikr_k}}{r_k} - \frac{j}{4} \sum_{k=1}^{N_{TE}} a_k^{TE} H_0^{(2)}(p_k^{TE}\rho) - \frac{j}{4} \sum_{k=1}^{N_{TM}} a_k^{TM} H_0^{(2)}(p_k^{TM}\rho) \tag{3.23}$$

---

[1] that is complex in general and hence this method is called Complex Image Method

The first problem of this technique is that the extraction of the poles and the evaluation of the residue require a time consuming algorithm and, in addition, a large number of Image is needed to have the correct evaluation of the Green's Function. The second problem is that the Hankel functions introduces not physical near-field singularities even when the field point and source point are in different horizontal plane ($z \neq z'$).

Rational Fitting Function Method (RFFM)

$\tilde{G} - \tilde{G}_{as}$ is approximated in terms of rational functions using the Vector Fitting algorithm as

$$\tilde{G} - \tilde{G}_{as} \approx + \sum_{k=1}^{Nvf} \frac{a_k}{k_\rho^2 - p_k^2} \tag{3.24}$$

with the constrain $-\pi < arg(p_k) \leq 0$, in order to have only cylindrical waves with physical meaning.
Using the relation (3.22) we have

$$G \approx G_{as} - \frac{j}{4} \sum_{k=1}^{Nvf} a_k H_0^{(2)}(p_k \rho) \tag{3.25}$$

This technique solve the first problem of the DCIM because the Vector Fitting algorithm is very efficient and use less poles to have the correct approximation of the Green's function, but the second problem is still present because the Green's function is fitted with Hankel functions without any constrain in the case $\rho \to 0$ with $z \neq z'$.

Total Least Square Method (TLSM)

$\tilde{G} - \tilde{G}_{as}$ is approximated as a fraction of two polynomials

$$\tilde{G} - \tilde{G}_{as} \approx \frac{\tilde{P}^{(M-2)}(k_\rho^2)}{\tilde{Q}^{(M)}(k_\rho^2)} \tag{3.26}$$

where $\tilde{P}^{(M-2)}(k_\rho^2)$ and $\tilde{Q}^{(M)}(k_\rho^2)$ are polynomial in the variable k_ρ^2 of degrees $M - 2$ and M, respectively. Using the Total Least Square Technique the pole and the residual of $\tilde{G} - \tilde{G}_{as}$ are founded and we can write

$$\tilde{G} - \tilde{G}_{as} \approx \sum_{k=1}^{Ntls} \frac{a_k}{k_\rho^2 - p_k^2} \tag{3.27}$$

hence finally we have

$$G \approx G_{as} - \frac{j}{4} \sum_{k=1}^{Ntls} a_k H_0^{(2)}(p_k\rho) \tag{3.28}$$

This technique solve all the problems of the DCIM, indeed the TLSM use less poles of the RFFM with a minor computational cost and the choice of use two polynomial of degrees $M-2$ and M, impose that $G - G_{as} \to 0$ when $\rho \to 0$, solving the second problem.

3.2.2 The Quasi Static Green's function G_{as}

All the approaches described above needed of the extraction of the Quasi Static Green's function [35], this term dominate the near field interaction ($\rho \to 0$) and can be founded from the Spectral Domain Green's function in the limits $k_\rho \to \infty$. This terms give an analytical approximation of the Green's function for the low frequency and low distance usable to simplify the numerical code in many practical case. Here we consider only the Green's functions when $z > 0$ and $z' > 0$ (3.14),(3.15), because are used in the microstrip case, for the general case see [28].
If $k_\rho \to \infty \Rightarrow k_{z0} \approx k_{zr}$ we have

$$r_{TE} \to 0; \quad r_{TM} \to K = \frac{1-\varepsilon_r}{1+\varepsilon_r};$$

$$R_{TE} \to R_{TE0} = -e^{-i2k_{z0}t}; \quad R_q \to R_{q0} = \frac{K(1-e^{-i4k_{z0}t})}{1-Ke^{-i2k_{z0}t}}$$

then

$$\tilde{G}_{Aas}^{xx}(k_\rho; z > 0|z' > 0) = \frac{1}{2ik_{z0}}\left[e^{-ik_{z0}|z-z'|} + R_{TE0}e^{-ik_{z0}(z+z')}\right] \tag{3.29}$$

$$\tilde{G}_{\varphi as}(k_\rho; z > 0|z' > 0) = \frac{1}{2ik_{z0}}\left[e^{-ik_{z0}|z-z'|} + (R_{TE0} + R_{q0})e^{-k_{z0}(z+z')}\right] \tag{3.30}$$

in the Spatial Domain [2] we have

$$G_{Aas}(\rho; z, z') = \frac{1}{4\pi}\frac{e^{-ikr}}{r} - \frac{1}{4\pi}\frac{e^{-ikr_1}}{r_1} \tag{3.31}$$

$$G_{\varphi as}(\rho; z, z') = \frac{1+K}{4\pi}\frac{e^{-ikr}}{r} + \frac{K^2-1}{4\pi}\sum_{n=1}^{\infty}K^{n-1}\frac{e^{-ikr_n}}{r_n} \tag{3.32}$$

where $r = \sqrt{\rho^2 + (z-z')^2}$ and $r_n = \sqrt{\rho^2 + (z+z'+2nt)^2}$

---

[2]remember that $\sum\limits_{k=1}^{\infty} x^k = \frac{1}{1-x}$ if $|x| < 1$

3.2.3 The Static Green's function g_φ

From the Quasi Static Green's Function (3.32) is simple derive the static Green's function for the transverse problem of fig.3.2 (b)

$$g_\varphi(s, s') = \frac{1+K}{2\pi} \log(\sqrt{(y-y')^2 + (z-z')^2}) +$$

$$+ \frac{K^2-1}{2\pi} \sum_{n=1}^{\infty} K^{n-1} \log(\sqrt{(y-y')^2 + (z-z'+2nt)^2}) \qquad (3.33)$$

The singular part of the Static Green's function is:

$$g_{\varphi S}(s, s') = \frac{1+K}{2\pi} \log(\sqrt{(y-y')^2 + (z-z')^2}) \qquad (3.34)$$

3.2.4 The shape functions

We consider the case of fig.3.2 (b), on the conductor contour l_1 we choose N_1 point $s_{11}, s_{12}, \cdots \cdots, s_{1N_1}$ and N_2 point $s_{21}, s_{22}, \cdots \cdots, s_{2N_2}$ on the conductor countor l_2 then $l_1 = \bigcup_h L_{1h}$ and $l_2 = \bigcup_h L_{2h}$ where L_{1h} is the piece of contours between s_{1h} and $s_{1(h+1)}$ (similarly for L_{2h}) and define $N_1 - 1$ pulse functions u_{1h} like that $u_{1h}(s_1) = 1$ if $s_1 \in L_{1}h$ and $u_{1h} = 0$ otherwise (similarly for the second conductor) then we have

$$F_1'(s_1) = \sum_{h=1}^{N_1} f_{1h} u_{1h}(s_1) \quad F_2'(s_2) = \sum_{h=1}^{N_2} f_{2h} u_{2h}(s_2) \qquad (3.35)$$

On every point s_{1j} of the conductor 1 we can write the (2.41) as

$$\alpha_1 = \frac{1}{\varepsilon_0} \left(\oint_{l_1} g_\varphi(\mathbf{s}_{1j}; \mathbf{s}_n) \sum_{h=1}^{N_1} f_{1h} u_h(s_1) d\mathbf{s}_1 \right) + \frac{1}{\varepsilon_0} \left(\oint_{l_2} g_\varphi(\mathbf{s}_{1j}; \mathbf{s}_2) \sum_{h=1}^{N_2} f_{2h} u_h(s_n) d\mathbf{s}_2 \right)$$
$$(3.36)$$

similarly on point s_{2j} of the conductor 2:

$$\alpha_2 = \frac{1}{\varepsilon_0} \left(\oint_{l_2} g_\varphi(\mathbf{s}_{2j}; \mathbf{s}_n) \sum_{h=1}^{N_1} f_{1h} u_h(s_1) d\mathbf{s}_1 \right) + \frac{1}{\varepsilon_0} \left(\oint_{l_1} g_\varphi(\mathbf{s}_{2j}; \mathbf{s}_2) \sum_{h=1}^{N_2} f_{2h} u_h(s_n) d\mathbf{s}_2 \right)$$
$$(3.37)$$

Using the definition of the pulse functions we can write:

$$\alpha_1 = \frac{1}{\varepsilon_0} \sum_{n=1}^{2} \sum_{h=1}^{N_n} f_{nh} \left(\int_{L_{nh}} g_\varphi(\mathbf{s}_{kj}; \mathbf{s}_n) d\mathbf{s}_n \right) \quad for \quad j = 1; \cdots; N_1 \qquad (3.38)$$

$$\alpha_2 = \frac{1}{\varepsilon_0} \sum_{n=1}^{2} \sum_{h=1}^{N_n} f_{nh} \left(\int_{L_{nh}} g_\varphi(\mathbf{s}_{kj}; \mathbf{s}_n) d\mathbf{s}_n \right) \quad for \quad j = 1; \cdots; N_2 \qquad (3.39)$$

Defining the vectors
$\boldsymbol{\alpha}_1 = \alpha_1 * ones(N_1, 1); \boldsymbol{\alpha}_2 = \alpha_2 * ones(N_2, 1)$
$\mathbf{f}_1 = [f_{11} f_{12} \cdots f_{1N_1}]^T; \mathbf{f_2} = [f_{21} f_{22} \cdots f_{2N_2}]^T;$

We can rewrite these equation in a more compact form

$$\varepsilon_0 \begin{bmatrix} \boldsymbol{\alpha}_1 \\ \boldsymbol{\alpha}_2 \end{bmatrix} = \begin{bmatrix} \mathbf{A}_{11} & \mathbf{A}_{12} \\ \mathbf{A}_{21} & \mathbf{A}_{22} \end{bmatrix} \begin{bmatrix} \mathbf{f}_1 \\ \mathbf{f}_2 \end{bmatrix} \tag{3.40}$$

with

$$\mathbf{A}_{mn} = \begin{bmatrix} a_{mn}(1,1) & a_{mn}(1,2) & \cdots & a_{mn}(1, N_{N_n}) \\ a_{mn}(2,1) & a_{mn}(2,2) & \cdots & a_{mn}(2, N_{N_n}) \\ \vdots & \vdots & \vdots & \vdots \\ a_{mn}(N_{N_m}, 1) & a_{mn}(N_{N_m}, 2) & \cdots & a_{mn}(N_{N_m}, N_{N_n}) \end{bmatrix} \tag{3.41}$$

where

$$a_{mn}(k, h) = \int_{L_{nh}} g_\varphi(s_{mk}; s_n) ds_n \tag{3.42}$$

These integrals can be evaluated with the midpoint integration rule if $m \neq n$ or $k \neq h$ in this case we have:

$$a_{mn}(k, h) = g_\varphi(s_{mk}; s_{nh})(s_{nh} - s_{n\,h+1}) \tag{3.43}$$

Due to the logarithmic behaviour of the Green's function is needed, instead, an analytical evaluation of the singular part of the diagonal terms of the matrices $\mathbf{A}_{mm}$. To do this we split the Green's function in the singular part $g_S(s_{mk}; s_m)$ and the remaining regular part $g_{\varphi R}(s_{mk}; s_m)$

$$a_{mm}(k, k) = \int_{L_{mk}} g_{\varphi S}(s_{mk}; s_m) ds_m + \int_{L_{mk}} g_{\varphi R}(s_{mk}; s_m) ds_m \tag{3.44}$$

The first part of the second term can be integrate analytically and we obtain

$$a_{mm}(k, k) = \left[\frac{1 + K}{2\pi} (1.5 - \log(dist(s_{mk}; s_{m\,k+1}))) + \tag{3.45} \right.$$

$$\left. + g_{\varphi R}(s_{mk}; s_{m\,k+1}) \right] dist(s_{mk}; s_{m\,k+1}) \tag{3.46}$$

where $dist(s_{mk}; s_{m\,k+1}) = \sqrt{(y_{mk} - y_{m\,k+1})^2 + (z_{mk} - z_{m\,k+1})^2}$
In order to impose the shape normalization (2.13), we impose

$$\sum_{m=1}^{N_m} f_{km} = 1 \quad for \quad k = 1; \cdots; N_c \tag{3.47}$$

Is simple generalise this approach at the case of N_c conductors, indeed, on every contours we can write

$$\alpha_k = \frac{1}{\varepsilon_0} \sum_{n=1}^{N_c} \sum_{h=1}^{N_n} f_{nh} \left(\int_{L_{nh}} g_{\varphi}(\mathbf{s}_{kj}; \mathbf{s}_n) d\mathbf{s}_n \right) \quad for \quad j = 1; \cdots; N_k \qquad (3.48)$$

3.2.5   The kernels

Due to the dielectric influence we have two different Green's function for the Vector and Scalar potentials hence, we have two different Kernels (2.32)-(2.33). In this configuration we can't find an analytical formulation for the kernel that may be evaluated numerically as follow.

$$H^{nk}(\zeta) = \frac{1}{c_k} \sum_{m=1}^{N_m} \sum_{p=1}^{N_p} G(\mathbf{s}_{nm}; \mathbf{s}_{kp}; \zeta) f_{nm} ds_{nm} ds_{kp} \quad if \quad \zeta \neq 0 \qquad (3.49)$$

where $f_{nm} = F_n(\mathbf{s}_{nm})$

$$H^{nk}(\zeta) = \frac{1}{c_k} (\mathbf{G}(\zeta) \mathbf{df}_n)^T d\mathbf{s}_k \quad if \quad \zeta \neq 0 \qquad (3.50)$$

where $d\mathbf{s}_n = [|s_{n1} - s_{n2}|, \ |s_{n2} - s_{n3}|, \cdots, |s_{n\,N_n-1} - s_{nN_n}|]^T$;
$\mathbf{df}_n = [(f_{n1} ds_{n1}), \ (f_{n2} ds_{n2}), \cdots, (f_{nN_n} ds_{nN_n})]^T$ and

$$\mathbf{G}(\zeta) = \begin{bmatrix} G(\mathbf{s}_{n1}; \mathbf{s}_{k1}; \zeta) & G(\mathbf{s}_{n1}; \mathbf{s}_{k2}; \zeta) & \cdots & G(\mathbf{s}_{n1}; \mathbf{s}_{kN_p}; \zeta) \\ G(\mathbf{s}_{n2}; \mathbf{s}_{k1}; \zeta) & \cdots & \cdots & G(\mathbf{s}_{n2}; \mathbf{s}_{kN_p}; \zeta) \\ \cdots & \cdots & \cdots & \cdots \\ G(\mathbf{s}_{nN_m}; \mathbf{s}_{k1}; \zeta) & G(\mathbf{s}_{nN_m}; \mathbf{s}_{k2}; \zeta) & \cdots & G(\mathbf{s}_{nN_m}; \mathbf{s}_{kN_p}; \zeta) \end{bmatrix} \qquad (3.51)$$

when $\zeta \to 0$ the Green's functions are singular and the integral need to be evaluated analytically.

$$G_A^S(\mathbf{s}_{nm}; \mathbf{s}_{km}; \zeta \to 0) = \frac{1}{4\pi} \frac{e^{-ikr}}{r} \qquad (3.52)$$

$$G_{\varphi}^S(\mathbf{s}_{nm}; \mathbf{s}_{km}; \zeta \to 0) = \frac{1+K}{4\pi} \frac{e^{-ikr}}{r} \qquad (3.53)$$

That are the same of the cylindrical case then the singular parts of the Kernels it may be proven to be

$$H_{IS}^{nk}(\zeta) = -\frac{1}{2a_k \pi^2} \ln(\zeta) \qquad for \quad \zeta \to 0 \qquad (3.54)$$

$$H_{QS}^{nk}(\zeta) = -\frac{1+K}{2a_k \pi^2} \ln(\zeta) \qquad for \quad \zeta \to 0 \qquad (3.55)$$

with $a_k = \dfrac{c_k}{\pi}$. This behaviour can be integrate analytically.

Then the regular parts can be computed as:

$$H_{IR}^{nk}(0) = \frac{1}{c_k} \left(\mathbf{G}_A^{Rxx}(0)\mathbf{df}_n \right)^T d\mathbf{s}_k \tag{3.56}$$

$$H_{QR}^{nk}(0) = \frac{1}{c_k} \left(\mathbf{G}_\varphi^R(0)\mathbf{df}_n \right)^T d\mathbf{s}_k \tag{3.57}$$

3.2.6   Some details on the use of the Green's function

When we write eq. (2.6) we use a Green's function derived for a stratified medium, we write the integral equation on the surface of the conductors then the use of this Green's function is equivalent to fill the conductor of a dielectric with the same permeability of the layer where it is. This is possible because the field inside the conductors is zero then we can put inside material without change the external solution.

3.3 The 1D propagation problem

3.3.1 The differential operator

We need to numerical solve the equations (2.14),(2.21),(2.28), (2.29). In order to approx the differential operator with an error of second order we consider two staggered mesh as showed in figure:
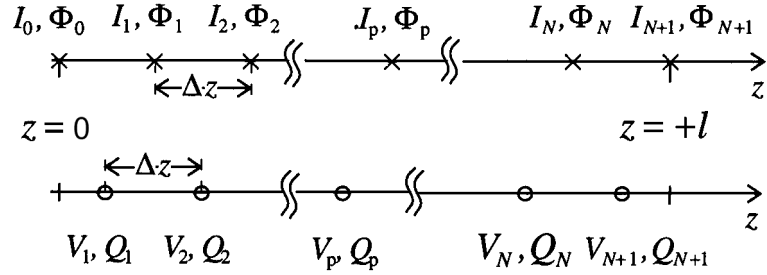
Figure 3.3: Staggered mesh

the numeric unknowns are

$$I_h = I(z_h^{(I)}) \qquad\qquad \Phi_h = \Phi(z_h^{(I)}) \qquad\qquad (3.58)$$

evaluated in the collocation points $z_h^{(I)} = +h\Delta z$ for $h = 1, 2, \ldots, N$
and

$$V_h = V(z_h^{(V)}) \qquad\qquad Q_h = Q(z_h^{(V)}) \qquad\qquad (3.59)$$

in the collocation points $z_h^{(V)} = +\left(h - \frac{1}{2}\right)\Delta z$ per $h = 1, 2, \ldots, N + 1$.
The boundary condition are the currents imposed at the ends of the line i.e.:

$$I_a = I_0 \text{ and } I_b = I_{N+1}$$

In order to discretize the differential operator we use the finite difference technique obtaining:

$$-D^{(V)}V = j\omega\Phi \qquad\qquad (3.60)$$

$$-D^{(I)}I = j\omega Q + \mathbf{b} \qquad\qquad (3.61)$$

where $\mathbf{I} = [I_1, \ldots, I_N]^T$, $\boldsymbol{\Phi} = [\Phi_1, \ldots, \Phi_N]^T$, $\mathbf{V} = [V_1, \ldots, V_{N+1}]^T$, $\mathbf{Q} = [Q_1, \ldots, Q_N]^T$;

the matrices $D^{(V)}$ and $D^{(I)}$, have dimension $N \times (N+1)$ and $(N+1) \times N$, respectively and are

$$D^{(V)} = \frac{1}{\Delta z} \begin{bmatrix} -1 & 1 & 0 & \cdots & 0 \\ 0 & \ddots & \ddots & \ddots & \vdots \\ \vdots & \ddots & \ddots & \ddots & 0 \\ 0 & \cdots & 0 & -1 & 1 \end{bmatrix} \text{ and } D^{(I)} = D^{(V)^T} \qquad (3.62)$$

the boundary conditions are take in account with the vector $\mathbf{b}$, defined as:

$$\mathbf{b} = \frac{1}{\Delta z} [-I_a, 0, \cdots, I_b]^T \qquad (3.63)$$

Now we need to discretize the integral equations (2.28), (2.29).

3.3.2 The first constitutive equation

We want to evaluate $\Phi_h = \Phi(z_h^{(I)})$ in the collocation points $z_h^{(I)} = +h\Delta z$ for $h = 1, 2, \ldots, N$. The mesh for $I(z)$ contain the extremes of integration, hence for compute the integral (2.28) is possible to use the trapezoid rule[3] of integration as follow:

$$\Phi_h = \int_0^{+l} H_I(|z_h^{(I)} - z'|)I(z')dz' = \int_0^{z_{h-1}} \cdot + \int_{z_{h-1}}^{z_{h+1}} \cdot + \int_{z_{h+1}}^{+l} \cdot \qquad (3.64)$$

The kernel $H_I(|\zeta|)$ have a singular behaviour of logarithmic type for $\zeta = 0$ then, the second integral need to be evaluated analytically, instead the first and the third integral can be evaluated with the trapezoid integration rule. The current is assumed piece-wise linear then:

$$I(z) = \begin{cases} \dfrac{I_h - I_{h-1}}{\Delta z}(z - z_h) + I_h & z_{h-1} \leq z \leq z_h \\ \dfrac{I_{h+1} - I_h}{\Delta z}(z - z_h) + I_h & z_h \leq z \leq z_{h+1} \end{cases}$$

The grid current contain the extreme of the line then this approximation can be used on all the line obtaining:

$$\mathbf{\Phi} = \mu M^{(f)}\mathbf{I} + \mu\mathbf{c} \qquad (3.65)$$

---

[3]this is the American term, the British term is trapezium rule

where:

$$
M_{hp}^{(f)} = \begin{cases} \dfrac{\Delta z}{2a\pi^2}\left(\ln\dfrac{2a}{\Delta z}+\dfrac{3}{2}+2a\pi^2 H_0\right) & \text{per } p=h \\[2ex] \Delta z\left[H(\Delta z)+\dfrac{1}{8a\pi^2}\right] & \text{per } p=h-1\geq 1 \text{ e } p=h+1\leq N \\[2ex] \Delta z\ H(|h-p|\Delta z) & \text{altrimenti} \end{cases}
$$

with $h=1,\cdots,N$, $p=1,\cdots,N$ and

$$
c_h = \begin{cases} \dfrac{1}{2}\Delta z H(\Delta z)I_0 + \dfrac{\Delta z}{8a\pi^2}I_0 + \dfrac{1}{2}\Delta z H[(N-1)\Delta z]I_{N+1} & \text{for } h=1 \\[2ex] \dfrac{1}{2}\Delta z H(\Delta z)I_0 + \dfrac{1}{2}\Delta z H[(N+1-h)\Delta z]I_{N+1} & \text{for } 2\leq h\leq N-1 \\[2ex] \dfrac{1}{2}\Delta z H[(N+1)\Delta z]I_0 + \dfrac{1}{2}\Delta z H[\Delta z]I_{N+1} + \dfrac{\Delta z}{8a\pi^2}I_{N+1} & \text{for } h=N \end{cases}
$$

3.3.3 The second constitutive equation

We want to evaluated the (2.29) in the collocation points $z_h^{(V)}=-l+\left(h-\frac{1}{2}\right)\Delta z$ for $h=1,2,\ldots,N+1$ we have:

$$
V_h = \frac{1}{\varepsilon}\int_{-l}^{l} H_Q(z_h^{(V)}-z')Q(z')dz' = \int_{-l}^{z_h^{(I)}}\cdot + \int_{z_h^{(I)}}^{z_{h+1}^{(I)}}\cdot + \int_{z_{h+1}^{(I)}}^{+l}\cdot \tag{3.66}
$$

for $h=2,\cdots,N$

The kernel $H_Q(|\zeta|)$ have a singularity of logarithmic type for $\zeta=0$ hence, the second integral need to be evaluated analytically instead, the first and the third can be evaluated using the mid point integration rule, because the mesh for $V(z)$ doesn't contain the extreme of integration. In the intervals $[z_1^{(V)},z_{N+1}^{(V)}]$ the charge is assumed piece-wise linear

$$
Q(z) = \begin{cases} \dfrac{Q_h-Q_{h-1}}{\Delta z}(z-z_h^{(V)})+Q_h & z_{h-1}^{(I)}\leq z\leq z_h^{(V)} \\[2ex] \dfrac{Q_{h+1}-Q_h}{\Delta z}(z-z_h)+Q_h & z_h^{(V)}\leq z\leq z_{h+1}^{(I)} \end{cases}
$$

instead in the interval $[z_1^{(I)},z_1^{(V)}]$ e $[z_{N+1}^{(V)},z_{N+1}^{(I)}]$ the charge is assumed piece-wise constant[4]:

$$
Q(z) = \begin{cases} Q_1 & 0=z_1^{(I)}\leq z\leq z_1^{(V)} \\[2ex] Q_{N+1} & z_{N+1}^{(V)}\leq z\leq z_{N+1}^{(I)}=l \end{cases}
$$

---

[4]note that we have an error that go to zero as Δz^2

Then we obtain

$$\mathbf{V} = \frac{1+K}{\varepsilon_0} M^{(V)} \mathbf{Q} \tag{3.67}$$

where:

$$M_{hp}^{(V)} = \begin{cases} \dfrac{7\Delta z}{16a\pi^2}\left(\ln\dfrac{4a}{\Delta z} + \dfrac{15}{16} + \dfrac{16a\pi^2}{7}\dfrac{H_{Q0}}{1+K}\right) & \text{per } p = h = 1 \text{ e } p = h = N+1 \\[2ex] \dfrac{3\Delta z}{8a\pi^2}\left(\ln\dfrac{4a}{\Delta z} + \dfrac{7}{6} + \dfrac{8a\pi^2}{3}\dfrac{H_{Q0}}{1+K}\right) & \text{per } p = h = 2, \cdots, N \\[2ex] \Delta z\left[\dfrac{H_Q(\Delta z)}{1+K} + \dfrac{1}{16a\pi^2}\left(\ln\dfrac{4a}{\Delta z} + \dfrac{1}{2}\right)\right] & \text{per } p = h+1 \\[2ex] \Delta z\,\dfrac{H(|h-p|\Delta z)}{1+K} & \text{per } p \geq h+2, N-2 \end{cases}$$

Remain to compute $V(0)$ e $V(l)$ because are not included in the mesh for $V(z)$.

$$V(0) = \frac{1}{\varepsilon_0}\int_{-l}^{l} H_Q(z')Q(z')dz' \tag{3.68}$$

$$V(l) = \frac{1}{\varepsilon_0}\int_{-l}^{l} H_Q(l-z')Q(z')dz' \tag{3.69}$$

$$\tag{3.70}$$

using the mid-point integration rule we obtain:

$$V(0) = \frac{1}{\varepsilon_0}\sum_{i=1}^{N+1} Q_i H_Q\left[\left(i-\frac{1}{2}\right)\Delta z\right]\Delta z \tag{3.71}$$

$$V(l) = \frac{1}{\varepsilon_0}\sum_{i=1}^{N+1} Q_i H_Q\left[l-\left(i-\frac{1}{2}\right)\Delta z\right]\Delta z \tag{3.72}$$

$$\tag{3.73}$$

3.3.4 Numerical solution

Now is possible to compute the current unknown, using equations (3.60),(3.61),(3.65) and (3.67) we have:

$$\left[D^{(V)}M^{(V)}(D^{(V)})^T - k^2 M^{(I)}\right]\mathbf{I} = \mathbf{d} \tag{3.74}$$

where

$$d = D^{(V)} M^{(V)} \mathbf{b} + k^2 \mathbf{c} \qquad (3.75)$$

is a known terms that take in account the boundary conditions.
Hence we have:

$$\mathbf{I} = inv \left(\left[D^{(V)} M^{(V)} (D^{(V)})^T - k^2 M^{(I)} \right] \right) \mathbf{d} \qquad (3.76)$$

This method use as boundary condition the terminal currents, is simple rewrite the algorithm in order to use the terminal voltages as boundary condition.

Chapter 4

ETL for cylindrical cables, numerical result

In this section, we consider two ideal conductors in the vacuum space (see fig.4.1). This example exhibits a lot of phenomena which can be found also in more complex applications as the microstrip case. Some benchmark with commercial code (NEC simulator) and with an analytical solution [11] are provide.
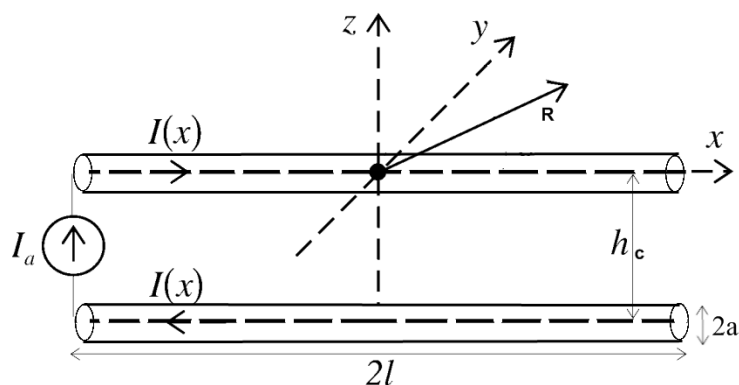
Figure 4.1: Cylindrical cable

When the transverse dimension of the structure is comparable with the wavelength the STL model doesn't give correct result and a very expensive fullwave solution is, in principle, needed. We will show that the ETL solution produce the correct behaviour of the structure with a computational cost similar at the STL model.

4.1   The shape function and the Kernel behaviour

Here we focus our attention on the influence of the proximity effect on the behaviour of the shape functions and the kernels. In Figure 4.2 is show the behaviour of $F_1(\theta)$ (3.5) for $a = 1mm$ and for different values of the ratio h_c/a. When h_c/a is very large, the proximity effect is negligible and the shape distribution is uniform $F_1(\theta) = \frac{1}{2\pi a}$, for small values of h_c/a (say < 10) this distribution differs significantly from the uniform case because the proximity effect is not negligible. In fig.4.3 the kernel behaviour for different value of h_c/a and kh_c is showed. We can observe the influence of the proximity effect on the kernel and that the kernel tend to have a quasi-impulsive behaviour when kh_c have a low value.
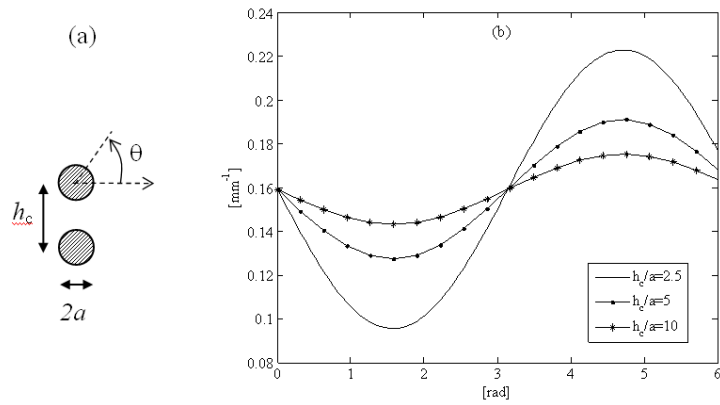
Figure 4.2: Cylindrical case, shape function
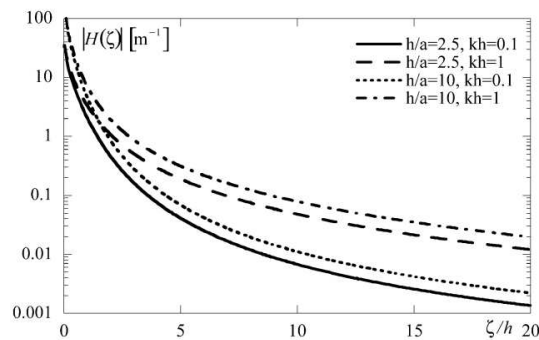
Figure 4.3: Kernel behaviour

4.2 Current distributions

The first reference case is a lossless interconnect with $l = 0.1$ m, $h = 10$ mm, and $a = 1$ mm, this case is compared with a full wave solution obtained from the NEC simulator and with the STL solutions. In fig.4.4 and 4.5 the current distributions predicted by the STL and ETL models have been compared with those obtained by the NEC simulator obtaining a satisfactory accordance, $I_a = 1$ is unitary and the far end is open (see fig. 4.1).
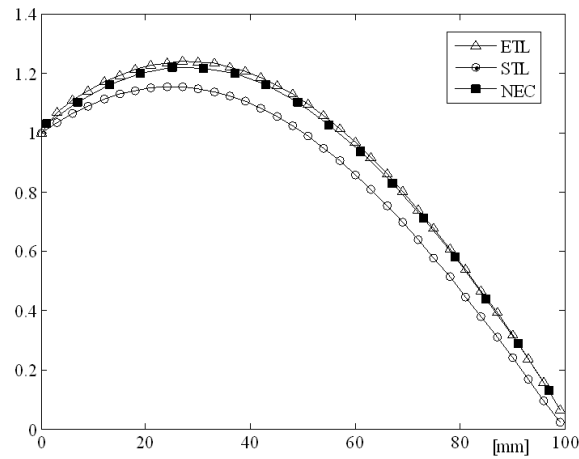
Figure 4.4: Case 1, amplitude (in arbitrary units) of the current distribution for open far end, at 1 Ghz
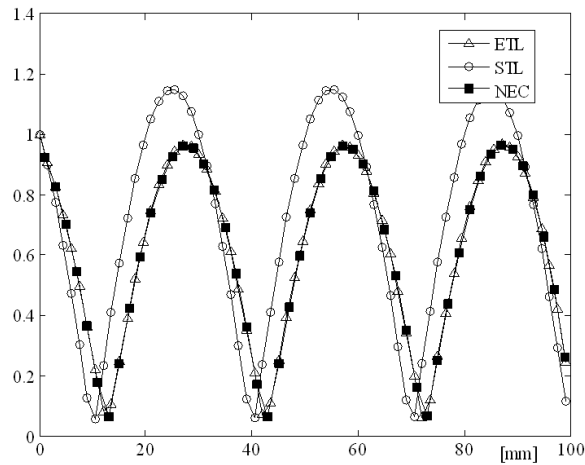
Figure 4.5: Case 1, amplitude (in arbitrary units) of the current distribution for open far end, at 5Ghz

In fig.4.6 we compute the difference between the currents distribution obtained from the STL and ETL models. For low frequencies, that is, $kh \leq 1$, there is a good agreement between STL and ETL models ($|I(x) - I_{STL}(x)| <$ 10% of $|I_a|$), whereas for $kh \approx 1$ there is a significant difference ($|I(x) - I_{STL}(x)| >$ 80% of $|I_a|$) because in this condition the transverse dimensions of the structure are comparable with the wavelength hence the STL model doesn't give the correct behaviour.
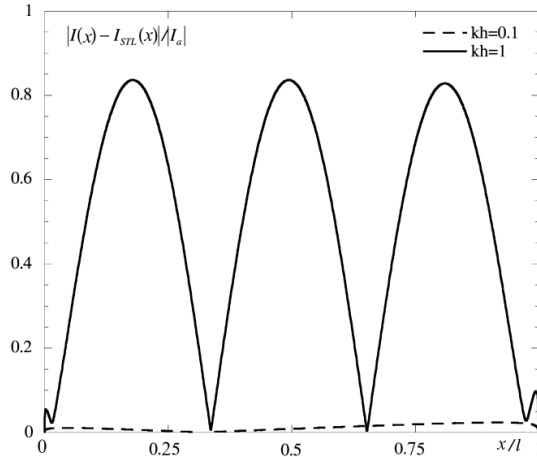
Figure 4.6: Spatial distribuzion of $|I(x) - I_{STL}(x)|/|I_a|$ for $kh_c = 0.1$ and $kh_c = 1$

The second test case that we have study is wire pair with $l = 1$ m, $h =$ 5.7 mm, and $a = 2.5$ mm. The line is fed at one end by a voltage source of 1V and is terminated on a short circuit at the other end. This case has been analyzed in [11] where a full-wave solution is provided by using the wire antenna theory. The proximity effect is there taken into account by introducing a set of "equivalent" wires whose artificial electrical axes are positioned so to satisfy the static problem in the transverse plane. Figure 4.7 shows the current distribution at 1.2 GHz for this case, computed by means of ETL and STL models and compared to the quoted full-wave solution. An approximated ETL solution is also plotted, obtained by disregarding the proximity effect and hence assuming uniform distributions. The agreement from the complete ETL solution and the full-wave solution is satisfactory.
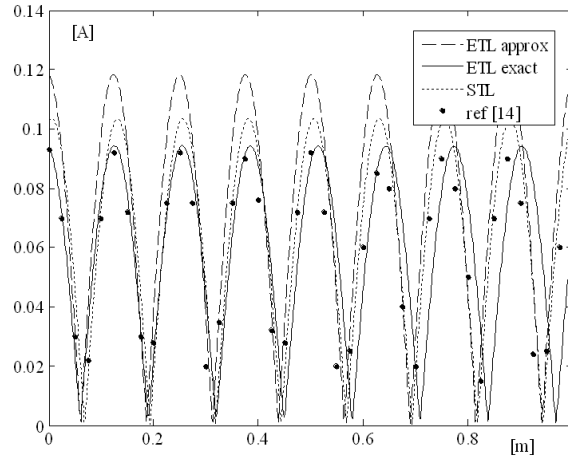
Figure 4.7: Case 2, amplitude of the current distribution computed at 1.2 GHz

4.3   Radiated power

The radial power flux density in the far field region, is given by (see fig.4.1)

$$S_R = \frac{\mu_0}{\varepsilon_0 8 \lambda R^2} |d(\theta, \phi)|^2 \tag{4.1}$$

$$d(\theta, \phi) = \sin\theta \left[1 - e^{-ikh\sin\theta\sin\phi} \right] \int_0^l I(x) e^{ikx\cos\theta} dx \tag{4.2}$$

The mean power radiated from the interconnect is given by

$$P_{rad} = \frac{\mu_0}{\varepsilon_0 8 \lambda} \int_0^{2\pi} d\theta \sin\theta \int_0^{\pi} d\phi |d(\theta, \phi)|^2 \tag{4.3}$$

We are considered two ideal wires, than the radiated power need to be feed from the terminations, in this case from the current generator I_a (see fig.4.1) then we have:

$$P_{rad} = Re\left(\frac{V_a I_a^*}{2}\right) - Re\left(\frac{V_b I_b^*}{2}\right) = Re\left(\frac{V_a I_a^*}{2}\right) \tag{4.4}$$

In fig.4.8 we compare the frequency behaviour of the P_{rad} computed with (4.3) and with (4.4). The agreement between the two curves is satisfactory with respect to the prediction of the position and amplitude of the resonances, but in correspondence with the minima of P_{rad}, $Re(\frac{V_a I_a^*}{2})$ is slightly negative. This unacceptable behaviour is due at the fact that we are characterising the interconnect as a two port, and hence, regardless of what is actually connected to

it, as pointed out in the paragraph 1.2 the Lorentz condition is not perfectly satisfied, the error is magnified when the feed current have a low value as we can see in fig.4.8 and fig. 4.9.
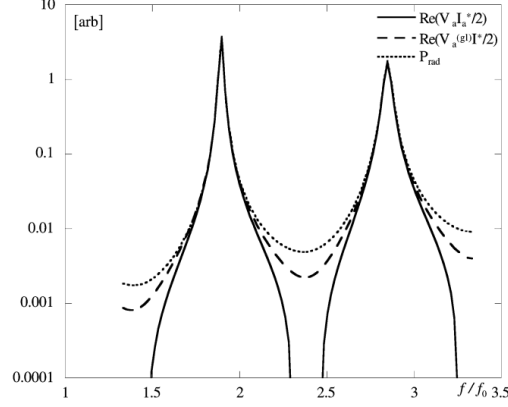
Figure 4.8: Case 1, Comparison between the frequency behaviour of the mean radiated power, $f_0 = 1.5$ GHz

A way to solve this problem is add the contribution of the four linear charge distributions

$$\Lambda_0^{(1)} = \frac{j}{\omega} \mathbf{J_s}(\mathbf{Q_1}) \cdot \hat{\mathbf{x}}\Big|_{x=0} \tag{4.5}$$

$$\Lambda_{+l}^{(1)} = \frac{j}{\omega} \mathbf{J_s}(\mathbf{Q_1}) \cdot \hat{\mathbf{x}}\Big|_{x=+l} \tag{4.6}$$

$$\Lambda_0^{(2)} = \frac{j}{\omega} \mathbf{J_s}(\mathbf{Q_2}) \cdot \hat{\mathbf{x}}\Big|_{x=0} \tag{4.7}$$

$$\Lambda_{+l}^{(2)} = \frac{j}{\omega} \mathbf{J_s}(\mathbf{Q_2}) \cdot \hat{\mathbf{x}}\Big|_{x=+l} \tag{4.8}$$

located, respectively, at the extremities of the two conductors on circumferences $\Gamma_0^{(1)}$ $\Gamma_{+l}^{(1)}$ $\Gamma_0^{(2)}$ $\Gamma_{+l}^{(2)}$ (see fig. 3.1) in order to satisfied the Lorentz condition. In fig.4.8 we also show the quantity $Re\frac{V_a^{(lg)}I_a^*}{2}$ obtained by evaluating the voltage distribution $V_a^{(lg)}$ as

$$V_a^{(lg)}(x) = j\frac{c}{k}\frac{d\Phi}{dx} \tag{4.9}$$

according to Lorentz gauge, evidently this new solution is not affected by the same problem. As showed in fig.4.9 the NEC solution predict the correct behaviour of the input impedance, also in correspondence of the minima, but it

can only solve the overall system including the terminal devices. The resonance frequencies of the ETL model and NEC are shifted to lower frequencies compared with those of STL model, which means that the interconnect described by the STL model appears electrically shorter than it actually is. Further,the amplitudes at the resonance frequencies are finite due to the spatial dispersion, and the maxima decrease with increasing frequency due to radiation losses. In figure 4.10 the radiation diagram of the structure for the case 1 is computed by the (4.2)
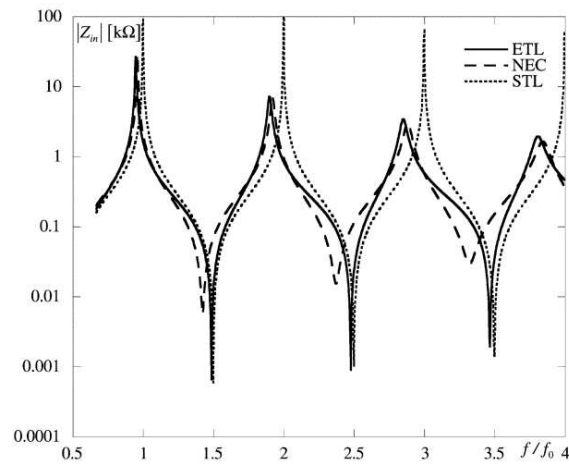
Figure 4.9: Case 1, comparison of the frequency behaviour of $|Z_{in}|$, $f_0 = 1.5$ GHz
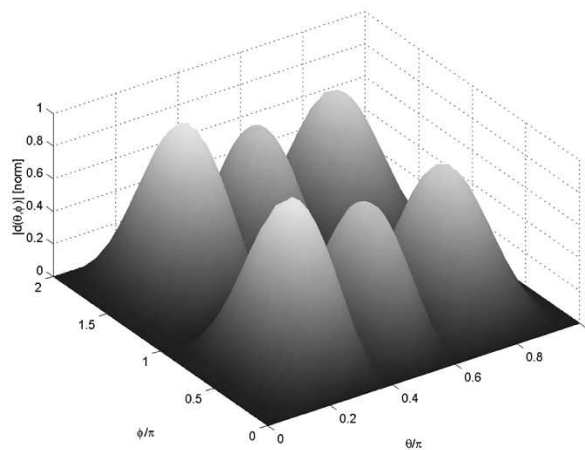
Figure 4.10: Case 1, radiation diagram of the i

4.4   Cylindrical wires, conclusion

In this section we have showed that the ETL model is able to predict the shift
of the resonance frequencies toward lower values which is typical of a lossy line
with frequency-dependent losses. Besides, the ETL model well predicts the
amplitudes at the resonance frequencies, that are finite and decreasing with
increasing frequency. In VLSI applications it is of great interest the study of
the proximity effect, because of the short distances between the signal traces
The kernel of the ETL formulation can take in account this effect, providing
the correct result. In conclusion, the ETL can compute the correct behaviour
of the interconnect without the numerical cost of the finite elements codes.

Chapter 5

ETL for coupled microstrip, numerical results

A structure of great interest for high-speed electronic applications is the microstrip line: Figure 5.1 (a) shows a simple example of a three conductor microstrip, made by two signal conductors on a dielectric layer and a ground plane. Figure 5.1 (b) shows the references for the voltages and currents (note that the grounded modes are considered).
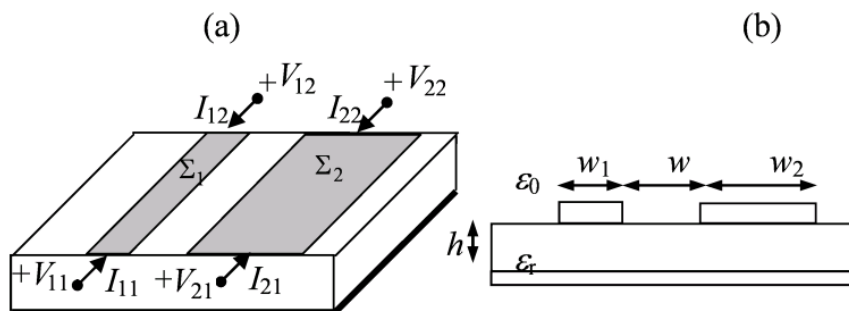
Figure 5.1: Coupled microstrip

In this section we'll analyse the behaviour of this kind of structure when the STL approximations fails, we'll show that the ETL code can reproduce the correct behaviour of the interconnects as the shift of resonance frequency at low value respect the prediction of the STL model or the radiation without the high computational cost typical of the finite elements code.

5.1   The shape function

In the section 4.1 we show that the shape function for two cylindrical cables are known analytically, in this case the shape functions are no longer known in analytical form.
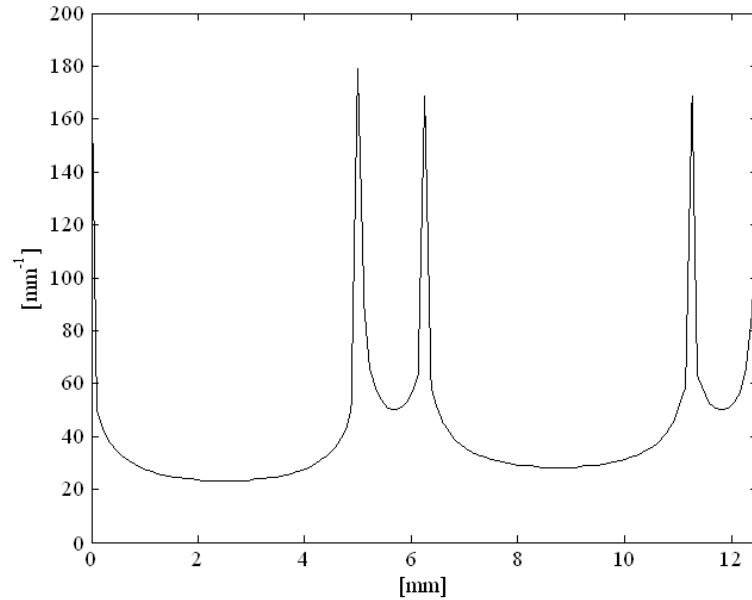
Figure 5.2: Numerically computed shape function for a microstrip

However they may be easily numerically computed by solving the electrostatic problem in the cross-section: for instance Figure 5.2 shows the computed behaviour of the shape function for the signal conductor of a single microstrip with $w_1 = 5mm$, $h = 8.7mm$, $\varepsilon_r = 4$ and with thickness $t = 1.25mm$. It is here evident the effect due to the sharp edges of the rectangular section.

5.2   The Green's functions

In this section we'll showed the Green Function behaviour for a microstrip and we'll show a good approximation of this function usable for the practical interconnect. As showed in the section 3.2.1 the Green Function can be split in two terms , a quasi-static term that is the only terms left when $f \to 0$ and that dominate the local range interactions, and the dynamic term that is associated to parasitic waves (surface waves, leaky waves), vanish as $f \to 0$ and dominate the long-range interactions.
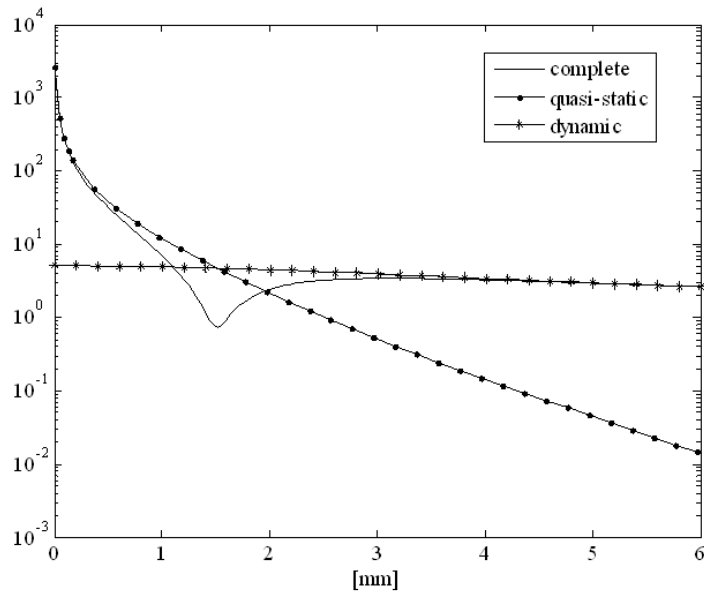
Figure 5.3: Scalar potential Green's function G_φ

Figure 5.3 gives an example of scalar potential Green's function G_φ computed at 2.1 GHz for a single microstrip with $\varepsilon_r = 4.0$, $h = 0.7mm$. The quasi-static term dominates the near-field region, whereas for increasing distances the dynamic terms become the principal ones. For the antenna problems is very important know the correct behaviour of the Green Function for large distance, because in this case is fundamental estimate the far field. Instead in practical interconnects, the quasy-static terms are dominant for a very large range of frequency, hence the approximation of the remainder is usually satisfactorily pursued by a low-order model. A reliable criterion [35] states that the Green functions are accurately represented by the quasi-static terms when $k_0 t \sqrt{\varepsilon_r - 1} < 0.1$, k_0 being the vacuum space wavenumber. The use of this approximation can reduce drastically the computational cost of the simulator.

5.3   Radiation and finite length effect

As case 1,we consider a PCB microstrip, with the geometry of Fig. 5.1, assuming a single signal conductor above a ground plane and a length of 36 mm. The signal conductor has zero thickness, width $w_1 = 1.8mm$ and lies on a FR-4 dielectric layer of thickness $h = 1.016mm$, dielectric constant $\varepsilon_r = 4.9$ and magnetic permeability $\mu = \mu_0$. The conductors and dielectric are assumed ideal.
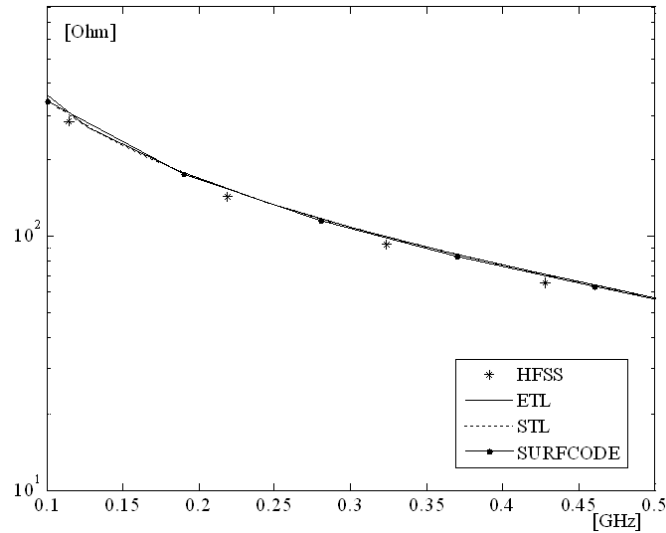
Figure 5.4: Case 1, absolute value of the input impedance in low frequency range

The ETL model solution is compared to the STL one and two 3D full-wave solutions, one provided by the commercial FEM code HFSS [39] and the other by the tool SURFCODE, which is based on the Electric Field Integral Equation formulation [26]. Assuming for this case $h_c = h$, since $\varepsilon_{reff} \approx 3.65$ we have $kh_c \approx 0.1$ at 1.4 GHz, which is in agreement with the results shown in Fig.5.5, where it is plotted the absolute value of the input impedance of the line with the far-end left open.
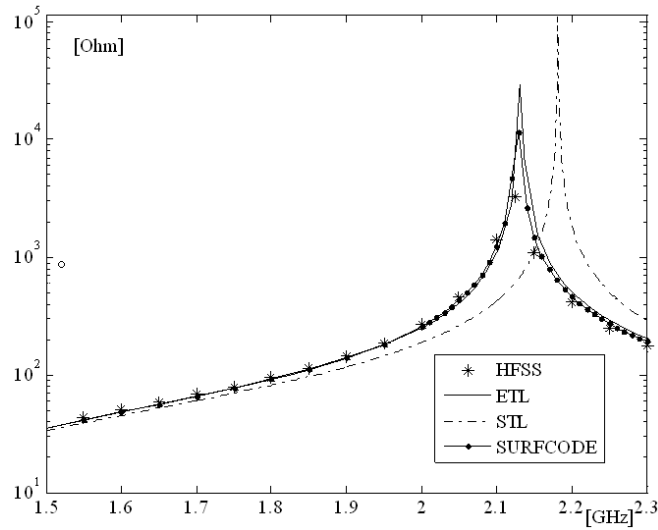
Figure 5.5: Case 1, absolute value of the input impedance in high frequency range

Indeed, the results of all the models agree satisfactorily in the low frequency range (Fig. 5.4), whereas in the high-frequency range the full-wave solutions start to deviate significantly from the ideal STL solution (Fig. 5.5) with a shift of the resonance frequency to low value which means that the interconnect described by the STL model appears electrically shorter than it actually is.

Further, the amplitudes at the resonance frequencies are finite due to the spatial due to dispersion, and the maxima decrease with increasing frequency due to radiation losses as see before in the cylindrical case.

Figure 5.6 shows the absorbed real power computed with $I_0 = 1mA$. The ETL solution is in good agreement with the full-wave one around the peak, whereas there is a deviation in the other ranges (where, however the values of power are very low). Note that, since we are in the ideal case, the STL input impedance is strictly imaginary, hence the absorbed real power predicted by the STL model is always zero.
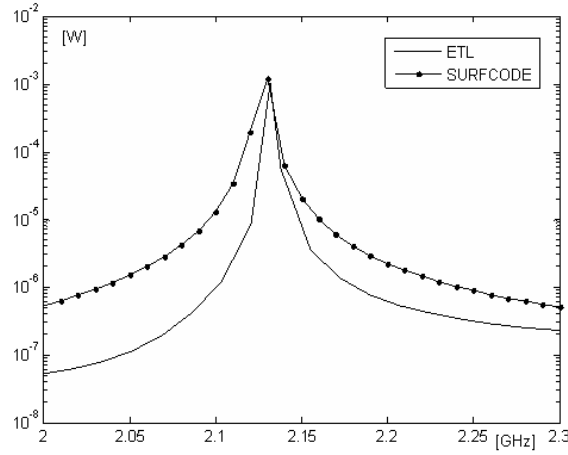
Figure 5.6: Case 1, absorbed real power
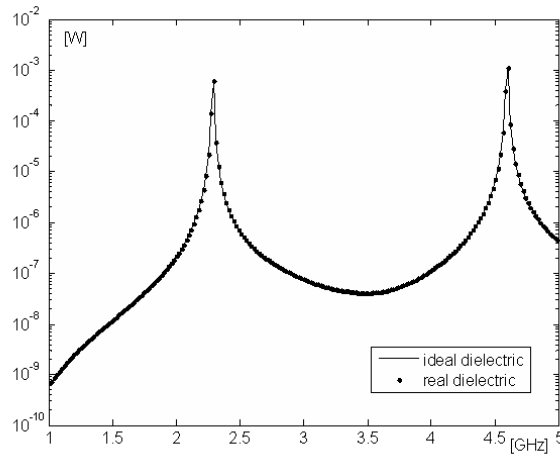
Figure 5.7: Case 1, absorbed real power with ideal and real dielectric

Let us now introduce a lossy dielectric described by the Debye model,

$$\varepsilon_r = \varepsilon_\infty + \frac{\varepsilon_{DC} - \varepsilon_\infty}{1 + i\omega\tau} \tag{5.1}$$

with $\varepsilon_\infty = 4.07$, $\varepsilon_{DC} = 4.178$ and $\tau = 1.15ps$. Fig.5.7 shows the dissipated power computed in the same conditions described for Fig.5.6, both considering a real and an ideal dielectric with $\varepsilon_r = \varepsilon_{DC} = 4.178$ It is clear that in this case the dielectric losses are negligible with respect to the losses associated to the other high-frequency phenomena.

5.4 Differential and common mode

As second case, let us consider the interconnect of Fig.5.1 with $w_1 = 5$ mm, $w_2 = 10$ mm, $w = 2.5$ mm, $h = 8.7$ mm , a total length of $l = 50$ mm and a conductor's thickness $t = 1.25$ mm We assume to be in the free space, hence $\varepsilon = \varepsilon_0$, $\mu = \mu_0$. This case is a particular case of microstrip structure, where the Green's function is known analytically using the image theorem, is important to note that this Green's function can be obtained from the 3.32 when $\varepsilon_r = 1$. For such a structure, a characteristic dimension in the transverse plane may be assumed as $h_c = 9.35$ mm i.e. the average value between h and the distance between the signal conductors. We investigate the range $(0.1 \div 3)$ GHz, corresponding to $kh_c \in (0.02 \div 0.59)$. Figg.5.8, 5.9 shows the frequency behaviour of the input impedance Z_{s1} [1] predicted by the ETL model and compared to the full-wave solution and the STL one. Fig.5.10 shows the frequency behavior of the transfer impedance Z_m . It can be clearly observed that the three models agree in the low frequency range, where the transverse dimensions of the interconnect are electrically short and hence the propagation is of quasi-TEM type. The standard TL solution gives a satisfactory prediction up to 0.5 GHz, corresponding to $kh_c \approx 0.1$. For higher frequencies the results of the STL model are inaccurate. The ETL model, on the contrary, agrees very well with the full-wave solution, both in reproducing the positions of the resonances and their peak values.
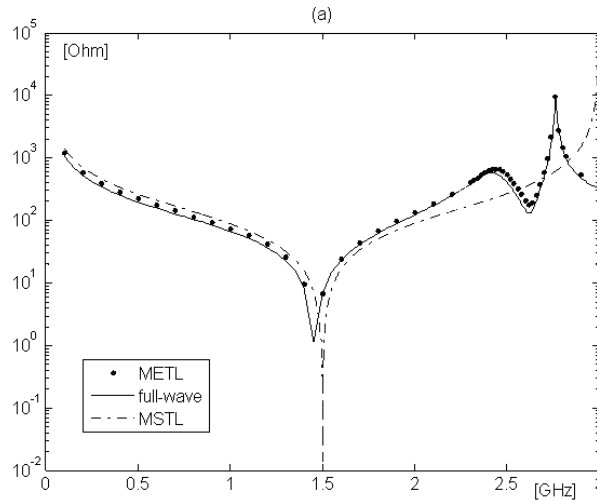
Figure 5.8: Case 2, absolute value of the input impedance $|Z_{s1}|$

---

[1] $Z_{s1} = V_{11}I_{11}$ when $I_{12} = I_{21} = I_{22} = 0$
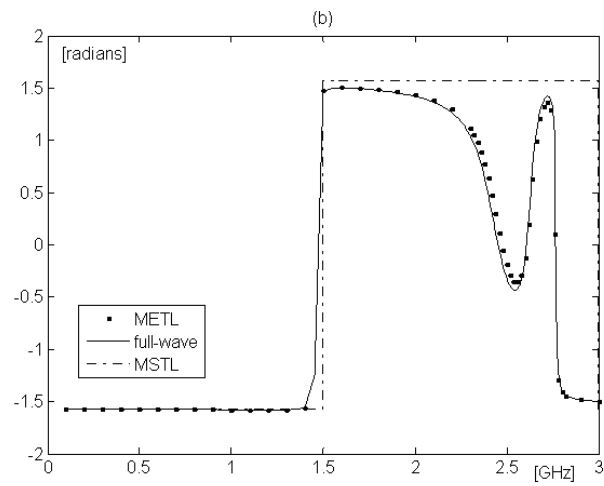
Figure 5.9: Case 2, phase of the input impedance $\angle Z_{s1}$
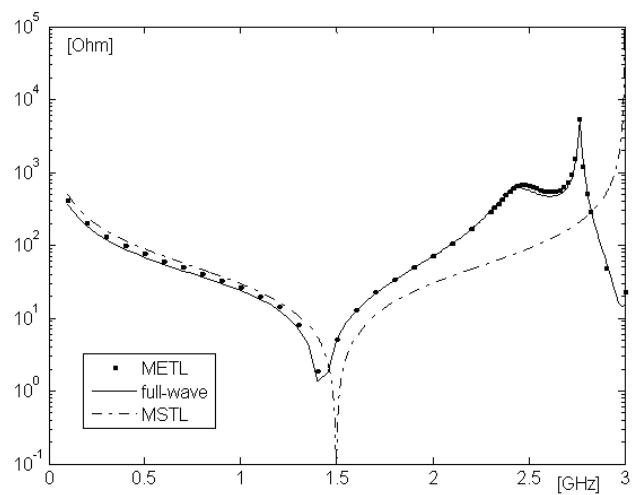
Figure 5.10: Case 2, absolute value of the transfer impedance $|Z_m|$

Similar considerations hold for the mixed-mode impedance matrix defined as in (2.49), whose entries are depicted in Fig.5.11, 5.12, 5.13.
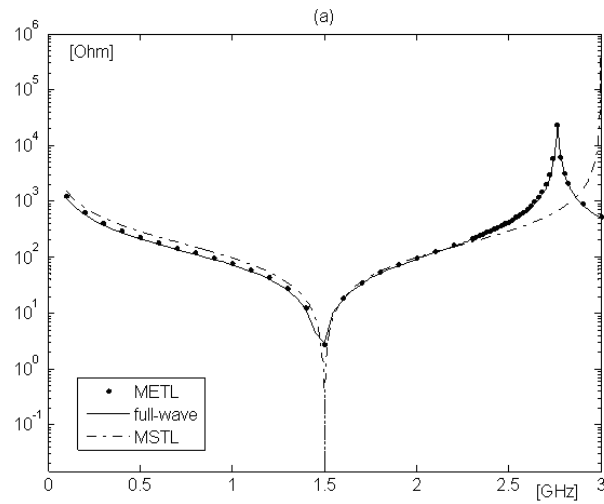
Figure 5.11: Case 2, Frequency behaviour of the absolute value of the mixed-mode impedance $|Z_{dd}|$
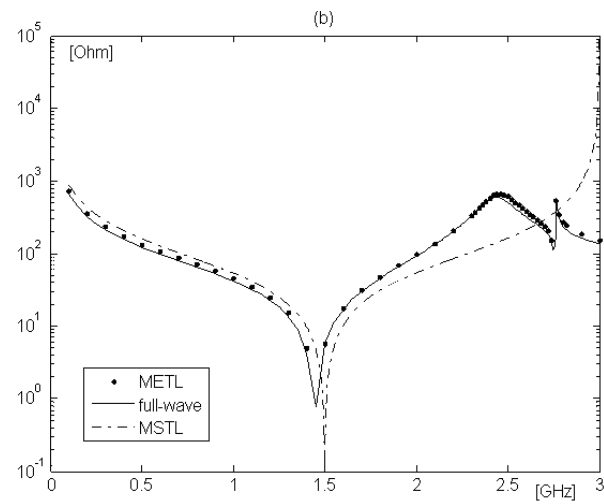
Figure 5.12: Case 2, Frequency behaviour of the absolute value of the mixed-mode impedance $|Z_{cc}|$
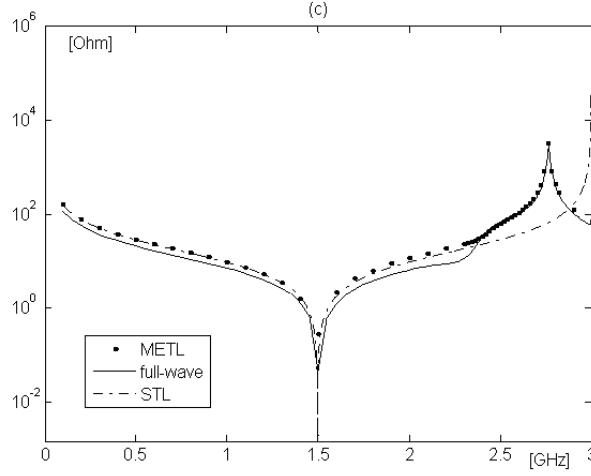
Figure 5.13: Case 2, Frequency behaviour of the absolute value of the mixed-mode impedance $|Z_{cd}|$

Let us now focus on the mixed-mode power balance. Let us assume the line to be fed at $x = 0$ by $I_d = I_{d1} = 1$ and $I_c = I_{c1} = 1$ (arbitrary units) and open at the far end. The active power delivered to the modes may be evaluated as

$$P_d = \frac{1}{2}\text{Re}\left\{V_{d1}I_{d1}^*\right\} = \frac{1}{2}\text{Re}\left\{Z_{dd}\right\} + \frac{1}{2}\text{Re}\left\{Z_{dc}\right\}$$

$$P_c = \frac{1}{2}\text{Re}\left\{V_{c1}I_{c1}^*\right\} = \frac{1}{2}\text{Re}\left\{Z_{cd}\right\} + \frac{1}{2}\text{Re}\left\{Z_{cc}\right\}$$

Assuming low frequencies ($kh_c \ll 1$) and symmetric structures ($Z_{cd} = Z_{dc} = 0$), since the conductors are ideal the active power must be zero. For symmetric structures with increasing frequency we may observe an increasing value of such a power, clearly related to the radiation loss which starts to become significant. The modes are decoupled in power and the power dissipated in radiation is related to the real parts of Z_{dd} and Z_{cc}. In the general case of asymmetric conductors, the power balance should include the fraction of the power converted from one mode to the other one, which is related to the real parts of Z_{cd} and Z_{dc} . Fig.5.14, 5.15 and 5.16, shows the frequency behaviour of the real part of Z_{dd} ,Z_{cc} and Z_{cd} . Note that the model proposed here is able to predict the radiation loss, whereas the standard transmission line does not include such phenomenon, hence it would always give $P_d = P_c = 0$.
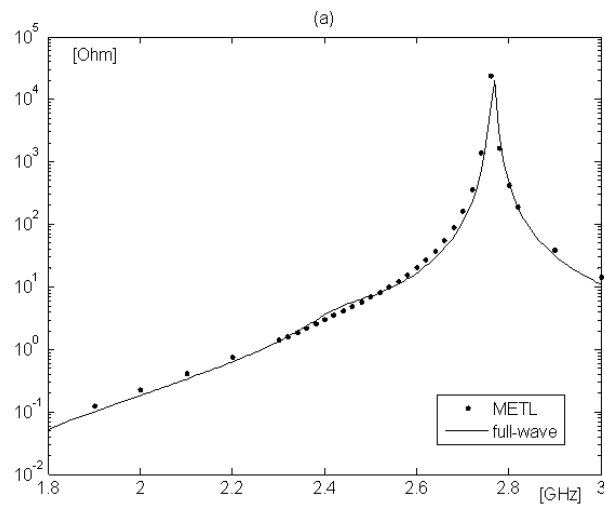
Figure 5.14: Case 2, Frequency behaviour of the real parts of Z_{dd}
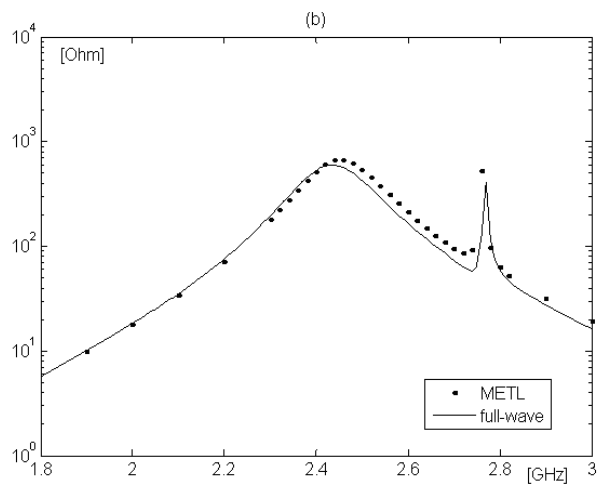
Figure 5.15: Case 2, Frequency behaviour of the real parts of Z_{cc}
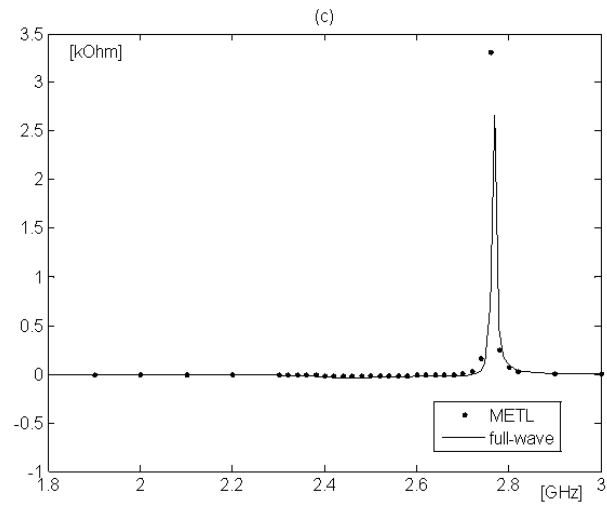
Figure 5.16: Case 2, Frequency behaviour of the real parts of Z_{cd}

For such structures it could be of interest to evaluate the scattering parameters in the high-frequency range. This is extremely useful for a correct interpretation of the experimental high-frequency characterisation of mixed-mode systems, as pointed out for instance in [17, 19]. For the mixed-mode scattering matrix, we adopt definition (2.68). Fig.5.17, 5.18 shows the frequency behaviour of the differential mode S_{dd} and S_{dc} the mode conversion parameter at port $1(z = 0)$.
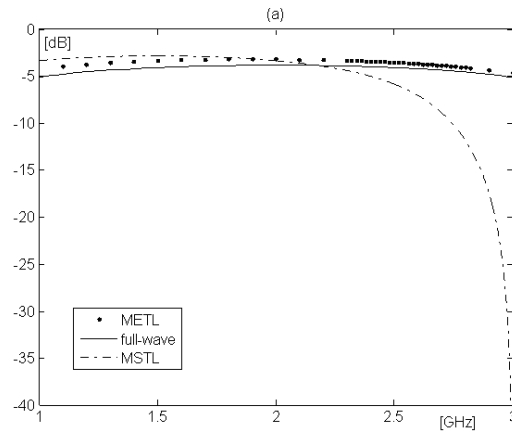
Figure 5.17: Case 2, Frequency behaviour of the mixed-mode S-parameters $|S_{dd}|$
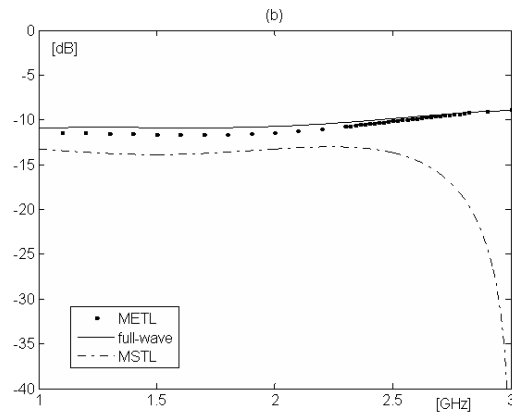
Figure 5.18: Case 2, Frequency behaviour of the mixed-mode S-parameters $|S_{dc}|$

Let us consider two cases, feeding the structure with a pure differential mode or with a pure common mode:

Case 1 $I_{d1} = 1(a.u.)$ and $I_{c1} = 0$
Case 2 $I_{d1} = 0$ and $I_{c1} = 1(a.u.)$
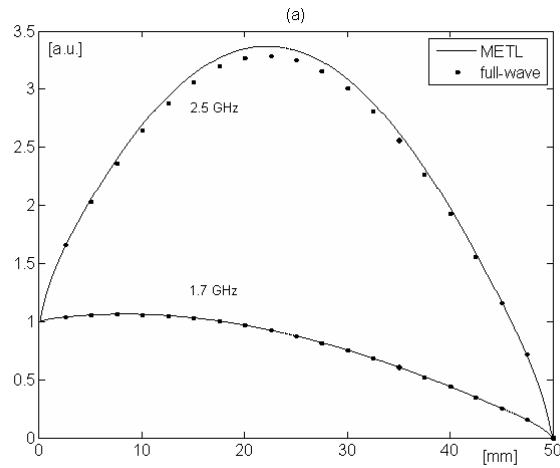
Figure 5.19: Case 2, Spatial distribution of the amplitude of the currents for two values of frequency $|I_d(x)|$ for a pure differential-mode feeding
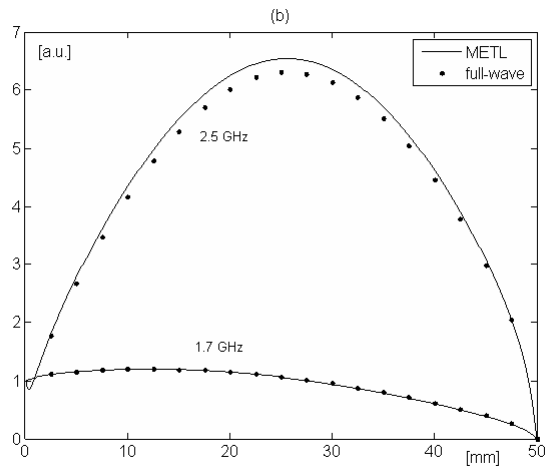
Figure 5.20: Case 2, Spatial distribution of the amplitude of the currents for two values of frequency $|I_c(x)|$ for a pure common-mode feeding
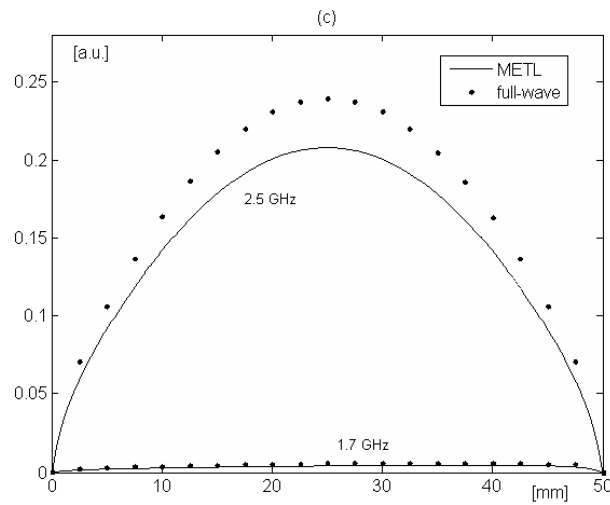
Figure 5.21: Case 2, Spatial distribution of the amplitude of the currents for two values of frequency $|I_c(x)|$ for a pure differential-mode feeding, normalized to the maximum of $|I_d(x)|$

The agreement at 1.7 GHz is excellent, whereas there is a difference in the distributions computed at 2.5 GHz. I have computed the distributions at 2.8 GHz which show an agreement similar to what obtained at 1.7 GHz. The difference at 2.5 GHz is probably due to the influence of the spurious resonance in the transverse plane observed around 2.4 GHz (see Figs.5.8 and 5.10), and the fact that the ETL model and the full-wave model treat in a different way the behaviour in the transverse plane.

5.5   Coupled microstrip, crosstalk

A third example is provided by a coupled microstrip made by two signal conductor and a ground plane. In this case (see Fig.5.1) we have considered $w_1 = w_2 = w = 1.8mm$, $h = 1mm$, $\varepsilon_r = 4.17$ and a total length of 36 mm. The line behaviour is investigated in the frequency range $(0 \div 6Ghz)$ GHz, so extending to values of kh_c high enough to expect inaccurate results from the STL model. Here a crosstalk analysis has been performed, by assuming line 1 (see references in Fig.5.1) to be fed at the near end by a unitary sinusoidal voltage source and open at far end. The near and far ends of line 2 are both terminated on open circuits. The Figures 5.22 and 5.23 shows the frequency behaviour of the near and the far end crosstalk voltage defined as V_{21}/V_{11} and $V_{22}/V11$, respectively. Note that in this case-study we have approximated the complete Green functions, considering only the contribution of the quasi-static term, which is again the dominant one. In fig.5.24 the mutual impedance obtained from the complete ETL model and with this approximation is compared, showing a good accordance.
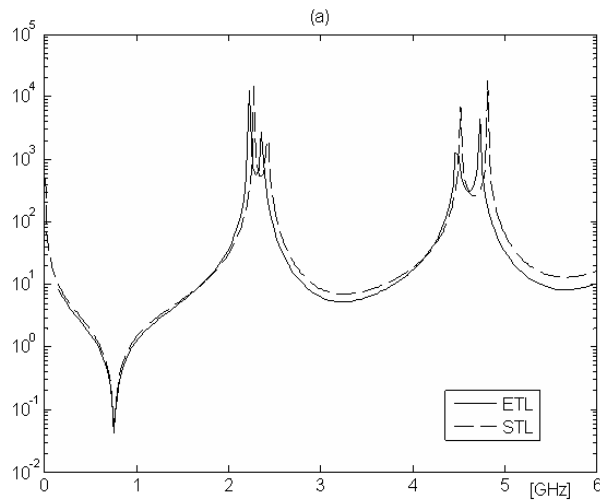
Figure 5.22: Case 3, Near end xtalk
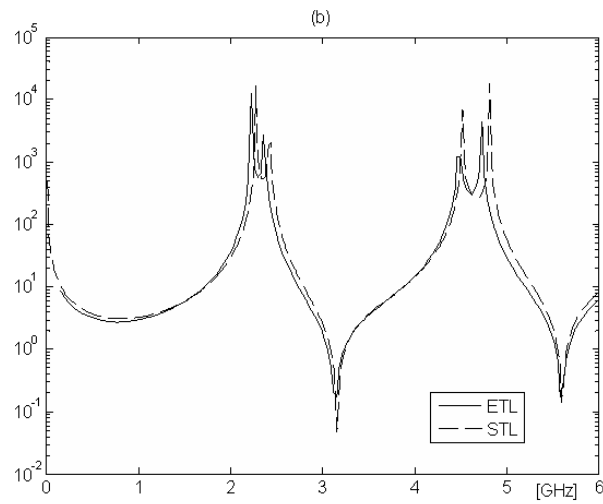
Figure 5.23: Case 3, Far end xtalk
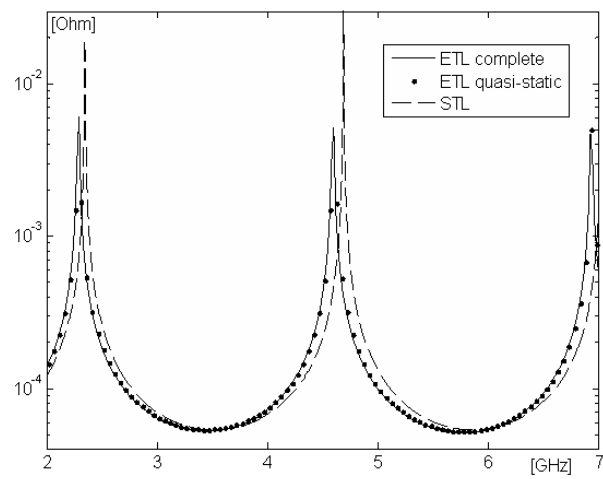
Figure 5.24: Case 3, Mutual impedance

5.6   Microstrip, conclusion

In this section we have showed the extension of the ETL model to study structure like microstrip. The dielectric media is included in the formulation using the Green's functions for layered media in order to reduce the computational cost of the model. An approximate version of the Green's Function (see paragraph 3.2.2), used in order to decrease furtherly this cost, is compared with the complete one showing that is usable in the case of interest. We have found again the behaviour see for the cylindrical cables the shift to low value of the frequency resonance and the amplitudes at this frequency are well predicts by the ETL model. In conclusion, the ETL can compute the correct behaviour of the interconnect used in the VLSI applications, without the numerical cost of the finite elements codes.

Conclusions and future works

In this Thesis, the extension of the popular transmission line model to high-speed VLSI interconnections is discussed. Starting from a full-wave integral formulation, an enhanced transmission line model is derived, able to describe interconnections with transverse dimensions comparable to the characteristic wavelength of the propagating signals. The model allows to describe, with a computational cost typical of a TL model, phenomenas which are not included in the solution of the classical TL model but could be only taken into account by a full-wave solution.

In Chapter 4, are showed some numerical results for two cylindrical cables in homogeneous media and this results are compared with numerical and analytical full-wave solutions, this is the start point of the thesis (for other details see the articles [23],[25],[24]).

In Chapter 5, are showed the principal results of this thesis, the numerical results for microstrip interconnections are compared with two numerical full-wave solutions, a good agreement is obtained.

As show in this Chapter, the principal advantage of the ETL model proposed in this thesis is the possibility of a qualitative study of the solution, indeed the Green's functions used in this work enable to separate the contribute of the guided modes from the contribute of unwanted modes and the formulation can evaluate correctly the radiation loss that is completely neglect in the STL model. This model can study the principal phenomenas of interest in the VLSI structures, like cross talk and the differential and common mode propagation. The results showed in this chapter are also published in the articles [42],[43], in Chapter 6 of the book *Transmission line models for high-speed conventional interconnects and metallic carbon nanotube interconnects* [44] and in the conference proceedings [45] - [51]

As future works, we'll remove from the ETL model the assumption of invariance of the interconnects along the x direction, in order to study for example the meander lines used in the VLSI interconnections to equalise the delay on different lines and we'll extend the ETL to take in account an external field.

Acknowledgements

Bibliography

[1] Whittaker E., "A History of the Theories of Aether and Electricity", *Harper and Brothers*: New York, 1960.

[2] Kirchhoff G., "On the Motion of Electricity in Wires", *Philosophical Magazine* XIII, p.393, 1857.

[3] Maxwell J.C., "A dynamical Theory of the Electromagnetic Field", *Proc. Roy. Soc.*, 13, pp.531-536, 1864.

[4] Ferraris G., "Sulla Teoria Matematica della Propagazione dellElettricit nei Solidi Omogenei", *Stamperia Reale*: Torino, Italy, 1872.

[5] Heaviside O., "Electromagnetic Theory", *E. and F.N. SPON LTD*: London, 1951.

[6] Lindell I.V. and Gu Q., "Theory of time-domain quasi-TEM modes in inhomogeneous multiconductor lines", *IEEE Transactions on Microwave Theory and Techniques*, 35, pp.893-897, 1987.

[7] Tkatchenko S., Rachidi F., Ianoz M., "Electromagnetic field coupling to a line of finite length: theory and fast iterative solutions in the frequency and time domain", *IEEE Trans. on Electr. Compatibility*, 37, pp.509-518, 1995.

[8] Larrabee D.A., "Interaction of an electromagnetic wave with transmission lines, including reradiation", *Proc. of IEEE Intern. Symp. Electromagnetic Compatibility.*, pp.106 -111, 1998.

[9] Haase H. and Nitsch J., "Full-wave transmission-line theory (FWTLT) for the analysis of three-dimensional wire like structure", *Proc. of Intern. Symposium on Electromagnetic Compatibilty*, EMC Zurich, 2001.

[10] Tkatchenko S., Rachidi F., Ianoz M., "High-frequency electromagnetic field coupling to long terminated lines", *IEEE Transactions on Electromagnetic Compatibility*, 43, pp.117-129, 2001.

[11] T.J. Cui , et al., "Full-wave analysis of complicated transmission-line circuits using wire models", *IEEE Trans. Antennas and Propag.*, 50, pp.1350-1359, 2002.

[12] Cui T.J., Chew W.C., "A Full-wave model of wire structures with arbitrary cross-sections", *IEEE Trans. on Electromagnetic Compatibility*, 45, pp.626-635, 2003.

[13] Haase H., Nitsch J., Steinmetz T., "Transmission-line super theory: a new approach to an effective calculation of electromagnetic interactions", *URSI Bulletin*, pp.33-59, 2003.

[14] Poljak D., Doric V., "Time-domain modeling of electromagnetic field coupling to finite-length wires embedded in a dielectric half-space", *IEEE Transactions on Electromagnetic Compatibility*, 47, pp. 247-253, 2005.

[15] Peterson A.F., Ray S.L. and Mittra R., "Computational methods for electromagnetics", *IEEE Press*: New York, 1998.

[16] King R.W.P., Fikioris G.J. and Mack R.B., "Cylindrical antennas and arrays", *Cambridge University Press*: New York, 2002.

[17] D. E. Bockelman, W.R. Eisenstadt, "Combined Differential and Common-Mode Scattering Parameters: Theory and Simulation", *IEEE Trans. on Microwave Theory and Tech.*, vol. 43, no. 7, pp.1530 - 1539, Jul. 1995.

[18] C. R. Paul, "A Comparison of the Contributions of Common-Mode Currents and Differential-Mode currents in Radiated Emissions", *IEEE Transactions on Electromagnetic Compatibility*, vol. 31, n.o. 2, pp.189 - 193, May 1989.

[19] K. M. Ho, K. Vaz and M. Caggiano, "Scattering Parameter Characterization of Differential Four-Port Networks using a Two-Port Vector Network Analyzer", *Proc. of 2005 Electronic Components and Technology Conference*, pp. 1846-1853.

[20] D.M. Hockanson, J.L.Drewniak, T.H.Hubing, T.P. van Doren, F. Sha and M.J.Wilhelm, "Investigation of fundamental EMI source mechanism driving common-mode radiation from printed circuit boards with attached cables", *IEEE Trans. on Electromagnetic Compatibility*, vol. 38, no. 4, pp.557 - 566, Nov. 1996.

[21] F.B.M. van Horck, A.P.J. van Deursen, P.C.T. van der Laan, "Common-mode currents generated by circuits on PCB - Measurements and

Transmission-Line Calculations", *IEEE Trans. on Electromagnetic Compatibility*, vol. 43, no. 4, pp.608 - 617, Nov 2001.

[22] I.F. Chen, C.M. Peng, C.W Hsue, "Circuit-concept approach to radiated emissions of printed circuit boards", *IEE Proc. Sci. Meas. Tech.*, vol. 151, no.3, pp.205 - 210, May 2004.

[23] Maffucci A., Miano G., Villone F., "Full-wave transmission line theory", *IEEE Trans. on Magnetics*, 39, pp.15931597, 2003.

[24] Maffucci A., Miano G., Villone F., "An enhanced transmission line for conducting wires", *IEEE Transactions on Electromagnetic Compatibility*, 46(4), pp.512-528, 2004

[25] Maffucci A., Miano G., Villone F., "An Enhanced Transmission Line Model for Conductors with Arbitrary Cross-Sections", *IEEE Transactions on Advanced Packaging*, 28(2), pp.174-188, 2005.

[26] Miano G., Villone F., "A surface integral formulation of Maxwell equations for topologically complex conducting domains", *IEEE Trans. on Antennas and Propag.*, 53(12), pp. 4001-4014, 2005.

[27] Miano G., Maffucci A., "Transmission lines and lumped circuits", *Academic Press*: New York, 2001.

[28] Ling Feng , V. Okhmatovski,B. Song, A. Dengi, "Systematic Extraction of Static Images From Layered Media Green's Function for Accurate DCIM Implementation" *Antennas and Wireless Propagation Letters*, vol. 6, pp.215 - 218,2007

[29] Collin R. E., "Foundation of Microwave Engineering", *Mc Graw-Hill*: New York, 1992.

[30] Paul C.R., "Analysis of Multiconductor Transmission Lines", *John Wiley and sons*: New-York, 1994.

[31] Pozar D. M., "Microwave Engineering", *John Wiley and sons*, 2004.

[32] Franceschetti G., "Electromagnetics", *Plenum Press*: New York 1997.

[33] H.A.Haus,J.R.Melcher, "Electromagnetic Fields and Energy", Prentice Hall,Englewood Cliffs,New Jersey,1989

[34] Michalski, K.A.; Mosig, J.R., "Multilayered media Green's functions in integral equation formulations", *IEEE Transactions on Antennas and Propagation*, 45(3), pp.508-519, 1997.

[35] Chow Y.L., Yang J.J., Fang D.G. and Howard G.E., "A closed-form spatial Green's function for the thick microstrip substrate", *IEEE Trans on Microwave Theory and Techniques*, 39, pp.588-592, 1991.

[36] Kourkoulos V.N. and Cangellaris A.C., "Accurate approximation of Green's functions in planar stratified media in terms of a finite sum of spherical and cylindrical waves", *IEEE Trans. Antennas and Propag.*, 54, pp.1568-1576, 2006.

[37] Boix, R. R.; Mesa, F.; Medina, F.,"Application of Total Least Squares to the Derivation of Closed-Form Green's Functions for Planar Layered Media",*IEEE Trans on Microwave Theory and Techniques*,27, pp.268-280 ,2005

[38] Burke G.J., Poggio A.J., "Numerical Electromagnetic Code (NEC) - Method of Moments", *Naval Ocean Systems Center*, Technical Document 116, 1981.

[39] http://www.ansoft.com/products/hf/hfss/

[40] "International Technology Roadmap For Semiconductors", Edition 2005, http://public.itrs.net

[41] A.G. Chiariello, A. Maffucci, G. Miano, F. Villone and W. Zamboni, "Electromagnetic Models for Metallic Carbon Nanotube Interconnects",*COMPEL*, Vol. 26, No. 3, pp. 571-585, June 2007.

[42] A.G. Chiariello, A. Maffucci, G. Miano, F. Villone and W. Zamboni, "A Transmission-line Model for Full-wave Analysis of Mixed-mode Propagation", in press on *IEEE Transaction on Advanced Packaging*.

[43] A.G. Chiariello, A. Maffucci, G. Miano, F. Villone and W. Zamboni, "High-frequency full-wave analysis of interconnects with inhomogeneous dielectrics through an enhanced transmission line model", in press on *ACES Journal*.

[44] Chapter 6: *Transmission line models for high-speed conventional interconnects and metallic carbon nanotube interconnects*, A.G. Chiariello, A. Maffucci, G. Miano, F. Villone, of the book: Eds. Farhad Rachidi and Sergei Tkachenko, *Electromagnetic Field Interaction with Transmission Lines, from Classical TL Theory to HF Radiation Effects* WITPRESS, Gran Bretagna.

[45] A.G. Chiariello, A. Maffucci, G. Miano, F. Villone, W. Zamboni, "Analysis of interconnects in huge frequency ranges with a 3-D superficial integral formulation" , *Proc. 9th IEEE Workshop on Signal Propagation on Interconnects*, Garmish-Partenkirchen, Germany, pp.89-92, ISBN $0 - 7803 - 9054 - 7$, 10-13 May 2005.

[46] A.G. Chiariello, A. Maffucci, G. Miano, F. Villone, W. Zamboni, "Signal integrity analysis of high-speed interconnects through a full-wave transmission line model", *Proc. 9th IEEE Workshop on Signal Propagation on Interconnects*, Garmish-Partenkirchen, Germany, pp.89-92, ISBN $0 - 7803 - 9054 - 7$, 10-13 May 2005.

[47] A.G. Chiariello, A. Maffucci, G. Miano, F. Villone, W. Zamboni, "Full-wave Numerical Analysis of Single-Layered Substrate Planar Interconnects", *Proc. 10th IEEE Workshop on Signal Propagation on Interconnects (SPI)*, Berlin, Germany, pp. 57-60, ISBN: 1-4244-0454-1, 9-12 May 2006.

[48] A.G. Chiariello, A. Maffucci, G. Miano, F. Villone, W. Zamboni, "Mode conversion on high-frequency signal propagation on asymmetric interconnects", *Proc. EMC Europe, 7th Inter. Symp. on Electromagnetic Compatibility*, Barcellona, Spain, pp. 365-370, ISBN: 84-689-9438-3, 4-8 settembre 2006.

[49] A.G. Chiariello, A. Maffucci, G. Miano, F. Villone, W. Zamboni, "Broad-Band Characterization of Conductors with Arbitrary Topology Using a Surface Integral Formulation", *Proc. 15th Electrical Performance of Electronic Packaging (EPEP)*, pp. 131-134, ISBN 1-4244-0668-4, 23-25 ottobre 2006.

[50] A.G. Chiariello, A. Maffucci, G. Miano, F. Villone, W. Zamboni, "Evaluation of Crosstalk in High-Frequency Interconnects with an Enhanced Transmission Line Model", *Atti della conferenza 15th Electrical Performance of Electronic Packaging (EPEP)*, pp. 91-94, ISBN 1-4244-0668-4, 23-25 ottobre 2006.

[51] A. G. Chiariello, A. Maffucci, G. Miano, F. Villone, W. Zamboni, "High-frequency full-wave analysis of interconnects with inhomogeneous dielectrics through an enhanced transmission line model", invited paper, *Proc. of ACES 2007, 23rd Annual Review of Progress in Applied Computational Electromagnetics*, pp.1483-1490, March 19-23, 2007, Verona, Italy

[52] A.G. Chiariello, A. Maffucci, G. Miano, F. Villone, W. Zamboni, "Metallic Carbon Nanotube Interconnects, Part I: a Fluid Model and a 3D Integral Formulation", *Proc. 10th IEEE Workshop on Signal Propagation on Interconnects (SPI)*, Berlin, Germany, pp.181-184, ISBN: 1-4244-0454-1, 9-12 May 2006.

[53] A.G. Chiariello, A. Maffucci, G. Miano, F. Villone, W. Zamboni, "Metallic Carbon Nanotube Interconnects, Part II: a Transmission Line Model", *Proc. 10th IEEE Workshop on Signal Propagation on Interconnects (SPI)*, Berlin, Germany, pp.185-188, ISBN: 1-4244-0454-1, 9-12 May 2006.

[54] A.G. Chiariello, A. Maffucci, G. Miano, F. Villone, W. Zamboni, "Electromagnetic Models for Metallic Carbon Nanotube Interconnects", *Proc. 12th IGTE Symposium*, Graz, Austria, ISBN-10: 3-902465-456-5, ISBN-13: 978-3-902465-56-6, pp. 7-12, 18-20 settembre 2006.

List of Figures